GEMINI

NEAR INFRARED CORONAGRAPHIC IMAGER

NICI

USER MANUAL

REVISION 0.80
1/19/05

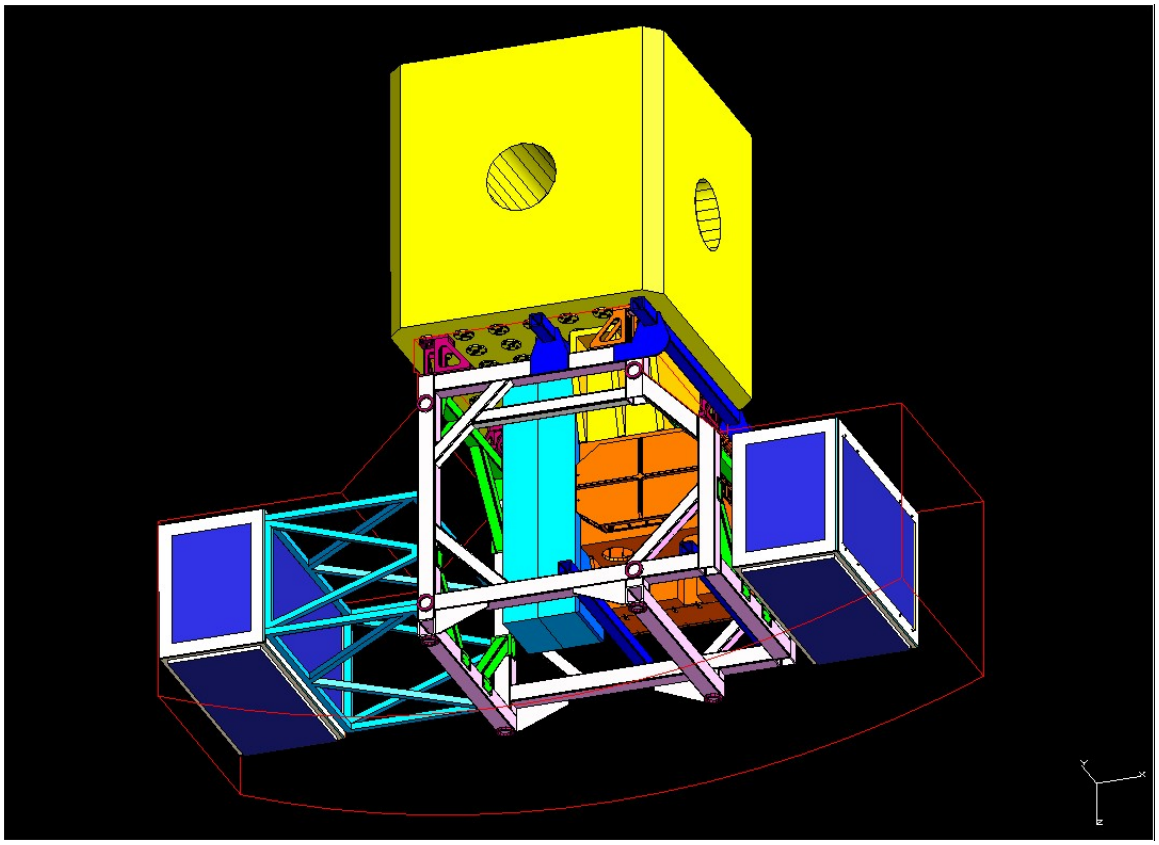

Revision History

Revision	Author	Summary of revisions	Date
0.80	D. Toomey Mike T	Prepared for preliminary 80% Release to Gemini.	1/19/05

Table of Contents

Table of Figures and Photos

1 Introduction

We stand on the brink of a new understanding of the Universe and of our place in it. After centuries of debate, speculation, and rhetoric, and after many false starts and erroneous claims, in our lifetimes a population of objects has been reliably and repeatably identified as extrasolar planets. In addition to these exciting and fundamental observations, we have obtained a few glimpses into the intermediate stages that link the birth of stars to the formation of planetary systems. We are poised now for the transition from discovery of these systems to their characterization. Our tools are marshaled for this transition. On the ground we have a new generation of large aperture telescopes equipped with advanced detectors and the atmospheric compensation systems needed to achieve diffraction limited imaging. In space we have established a major working observatory and have programs in various stages of completion to follow it with missions that will have even larger apertures, longer wavelength infrared imaging and higher astrometric accuracy. In the years to come there will be a significant array of instrumentation dedicated to the exploration and understanding of extra solar planetary systems.

In this document we describe Gemini's Near Infrared Coronagraphic Imager, NICI, a unique addition to this campaign. It is an imaging facility instrument, yet it has a narrowly focused purpose. From the very beginning, its design has been optimized to address this purpose with little compromise. Its goal is to extend our insight into the nature of this newly discovered planetary population by enabling deep imaging in circumstellar halos. This capability nicely complements the bias of radial velocity investigations for systems with high orbital velocities, highly inclined orbital planes, and periods not significantly exceeding the duration of the experiment. Moreover, it will be sensitive to symmetrically distributed material, disks characteristic of the emergence of young stellar objects, and the formation of mature planetary systems.

This document provides a description of the instrument and its components, and how to observe with NICI.

Section 2 provides a detailed description of the planned science projects.

Section 3 gives an overview of the NICI instrument and its capabilities

Section 4 describes important observational issues that are unique to NICI.

Section 5 describes operational issues and procedures that every observer should read.

Section 6 describes the operation of NICI through the Gemini software system.

Section 7 describes the engineering interfaces.

Section 8 describes setup and operation procedures.

Section 9 provides information on basic trouble shooting.

Section 10 defines acronyms and definition of terms used throughout this document.

Appendix A gives the detailed specifications of the filters and masks

1.1 Addendum Documents

The NICI User Manual has several documents that are included as Addendums. These addendums address the use and operation of parts of the NICI system.

- **NICI User Manual Addendum, Data Viewer (DV) Description**: A description of a tool used for viewing and manipulating images.
- **AO User Manual**: This manual describes the operation of the AO system through the engineering interface as well as remote operation as well as calibration procedures.
- **NICI IC Engineering Interface**: A manual that describes the engineering interface for the Instrument Control portion of NICI.

- **MKIR Array Controller Interface**: A description of the array control software and GUI for very specific array configuration and operation.

2 Science Description

2.1 Coronagraphic Imaging

Each astronomical instrument spans some domain of observational parameter space over which it can make useful observations. Experience has consistently shown that opening new windows into that space yields new and unanticipated science. Traditional venues for instrumental advances have involved enhanced sensitivity, or new domains of spatial and/or spectral resolution. In this proposal we describe an instrument designed to explore a new part of the sky, a region that has remained largely unobserved by direct means at any wavelength. The target is the halo region immediately surrounding the image of any source.

The few square arc seconds of the circumstellar halo occupy a small fraction of the sky, yet the halo region is disproportionately rich with astronomical importance and potential. It is here that the study of the circumstellar environment, from stellar birth to formation of mature planetary systems, lies hidden. It is here that the search for sub-stellar companions, brown dwarfs, and extra solar planets must proceed. And it is here, also, that the nature of the central regions of active galactic nuclei remains hidden. From our nearest neighbor stars to the brightest, most distant known objects, there is important science hidden beneath the glare of the circumstellar halo.

From the nearest stars to the furthest quasars, there are a host of significant astronomical questions that would also benefit from deep circumstellar imaging. For example, the nature of the low-mass end of the initial stellar mass function, and consequently the baryonic contribution to the mass of the universe, relies on characterizing the mass and distribution of brown dwarfs. If, as seems to be the case, stellar multiplicity extends to the brown dwarf population, then brown dwarfs in multiple systems could easily be under sampled. The evolution of close binary systems and the behavior of novae and supernovae could likewise be studied by deep imaging in the circumstellar region. The stellar halo can also become a significant factor in studying crowded fields like globular clusters, where the accumulated halos of many bright stars in the field can mask fainter sources. Similarly, the integrated point source halos of an extended object can prevent imaging fainter sources, as in the case of satellites near a planetary limb.

The detection and characterization of extra solar planetary systems is, in many ways, the archetypal circumstellar imaging problem, and is a fundamental piece of the search for who and what we are as a species. Ultimately, we wish to understand the frequency and nature of intelligent life in the universe, but there are significant gaps in our basic understanding of planetary systems. How are planets made and how are planet and star formation related? In what ways is the solar system typical or atypical of planetary systems? What determines where and if planets of a given type form, and where in the system they are ultimately observed? All phases of the evolution of planetary systems, from stellar birth to maturity, can be investigated via deep circumstellar imaging. The list of questions is long and the program to answer them is difficult and exciting. Many disciplines and instruments will be brought to bear on this problem, but imaging has always played a special role in the planetary community and is vital for separating stellar from circumstellar light.

In exploring the circumstellar environment, the stellar coronagraph has become the instrument of choice. It has become closely identified with the search for sub-stellar companions. Like Gemini, many of the world's major telescope programs have either built or planned a similar instrument. Two were added to the Hubble Space Telescope (STIS and NICMOS) and one has been built into the Advanced Camera for Surveys. These coronagraphs, however, were all designed as “add-ons” to an instrument designed and built to accomplish different science goals.

The coronagraph is indeed a powerful instrument, but the nature of that power has been largely misunderstood, partly because its action is governed by diffractive rather than geometric optics, but mostly because it is primarily an enabling instrument, particularly in ground-based systems. It cannot by itself, detect planets. When designed and used properly, it should allow the observer to achieve the long integrations and the accurate background subtractions needed to image at high dynamic range. Ultimately, as with any instrument, it is the skill of the observer in taking and reducing data that will determine the performance level of the instrument.

2.2 Origins and Coronagraphic Imaging

One of the earliest published references to the use of a coronagraph for a purpose other than observing the Sun was a paper on extra solar planet detection (Kenknight 1977). The suggestion was made to use a coronagraph for the detection of planets around other stars. In some sense, the close association of coronagraphic imaging with Origins Science began with this paper. The exciting discovery of a protoplanetary disk around the Star β-Pictoris (Smith and Terrile, 1984) crystallized the high level of interest in this kind of science and once again drew attention to the value of the coronagraph as a scientific tool. Reports from many review panels (c.f. Burke, 1992 and Elachi et. al., 1996) have stressed the importance of both the Origins Science program and the value of direct imaging to that effort. Those early reports focused primarily on the space-based imaging program because of the general impression that the turbulent atmosphere represented a fundamental limit to deep imaging. The atmosphere certainly remains an obstacle, but what true limit to imaging it represents is no longer clear. There are new telescopes and new technologies, but most of all there is human invention. The limit to what can be done from the ground has yet to be defined.

The present instrument is a milestone in circumstellar science. It is the first instrument to be designed solely for that purpose. It will be the only instrument of its kind to operate at a large telescope and be completely self-contained, with only the telescope between it and the sky. It is only fitting that it is driven by an ambitious and open-ended scientific agenda, and that it be designed to enable that human invention to the highest degree possible.

2.3 Young Stellar Objects

How stars and planetary systems form is one of the fundamental questions posed by NASA's Origins Program. Since protoplanetary disks form in the environments of Young Stellar Objects (YSOs), studies of the evolution and diversity of YSOs are essential to understanding the origin of planetary systems. There are regions in YSOs where key physical processes occur that shape the formation and evolution of stars and planets. Detection, resolution, and characterization of these regions will help answer many important questions.

The current paradigm for the birth of low mass stars (Adams, Lada and Shu 1987) is largely based on the interpretation of spectral energy distributions (SEDs) from near-IR to millimeter wavelengths. In the earliest stages, the in-falling, dusty molecular envelopes surrounding embedded protostars are completely opaque at wavelengths shorter than about 25 microns. This is known as a Class 0 SED. Within the infalling envelope, a star and nebular disk form. Most of the material destined for the star first falls onto the disk where it dissipates angular momentum and accretes onto the star. While gas is falling onto the star, an accretion-driven stellar or disk wind develops, which begins to clear envelope gas away from the rotational poles of the star-disk system, terminating the growth of the disk, and possibly establishing the eventual mass of the star as well. This is the embedded YSO stage, with a Class I SED, characterized by a spectrum that rises beyond two microns because almost all the light from the star is absorbed and reradiated by circumstellar dust at long wavelengths. In the most deeply embedded objects, most of the scattered light may come from walls of the outflow cavity in the envelope, giving a comet-like appearance to the circumstellar reflection nebulosity. The Class I stage is thought to last for at least a few times 10^5 years.

The in-falling envelope disperses, leaving an optically visible classical T-Tauri star (CTTS) with a circumstellar disk. Accretion through the disk slows as the star gains the final few percent of its mass. This Class II stage lasts from $10^6 - 10^7$ years, and is characterized by a spectrum that has IR emission in excess of photospheric values, but that is constant or falling longward of two microns. Accretion through the disk finally ends, due to lack of replenishment or disk gaps created by planet formation. The disk becomes optically thin, and the system evolves into a weak-line T Tauri star (WTTS). This stage is classified as Class III. If an optically thin protoplanetary or planetary debris disk remains, the stellar spectrum is that of a stellar photosphere with a small amount of mid- and far-IR excess arising from the disk. Since the IR emission from these disks is below the IRAS detection limits for nearby star-forming regions, there are currently only loose constraints on the timescale for dispersal of debris disks.

High-resolution near-IR (NIR) imaging of the circumstellar environments of YSOs complements information derived from SED modeling. It can provide direct observational confirmation at spatial scales that distinguish the morphology of circumstellar material spanning the full range of evolutionary states (ages $10^5 - 10^7$ yr).

With improvements in infrared instrumentation and telescope thermal control, and with the arrival of AO-correction on 8m-class telescopes, ground-based NIR imaging can achieve 0.06 arcsec diffraction-limited imaging at 2.2 microns, while observations with WFPC2 and NICMOS on HST achieve far-optical and NIR resolutions of 0.1 and 0.2 arcsec respectively. At these resolutions, structures as small as eight AU can be resolved in Taurus-Auriga (140 pc) and ρ-Ophiuchus (125 pc), the two nearest and best-studied star-forming regions. (See, for example, HST imaging by Padgett et al. 1999, and AO-corrected NIR imaging by Close et al. 1997).

From these studies, a consistent picture of YSO structure is beginning to emerge. Many Class I and Class II YSOs appear as conical-to-parabolic reflection nebulae crossed by dark lanes. The dark lanes are identified as circumstellar disks that currently are best seen edge-on, and which extend at right angles to known optical, NIR, and millimeter outflows in these objects. Bipolar reflection nebulae are identified as the in-falling envelopes illuminated by the central stars and, in some cases, the top and bottom surfaces of optically thick circumstellar disks. Typically, the envelopes have diameters of about 1000AU, and the disks have lengths of about 500AU with apparent thickness of order 100AU. These widths define surfaces with NIR optical depths of one, rather than the actual scale height.

The limb-brightened cavities seen in some objects are probably boundaries between the in-falling envelope and accretion-driven outflow (Figure 1). If so, the large opening angles of the cavities are in contrast to the narrowly collimated jets observed within the cavities of some objects. HH 30 in the Taurus molecular cloud (distance 140 pc) is the textbook example of a jet emerging from a YSO viewed edge-on. In this orientation, the problem of a bright central object is avoided because the disk itself occults it. Absent this effect, study of these disks at pole-on orientations is precluded. In the WFPC2 observations by Burrows et al. (1996), the emission-line jet is highly collimated and the FWHM of the unresolved jet is less than 20 AU (0.15 arcsec). It can be traced to within 30 AU of the obscured star. Its width is much narrower than the cleared cavity, so collimation must occur much closer to the star, in a region that is obscured by the edge-on disk. No-mask coronagraphic modes in NICI will permit imaging much closer to star.

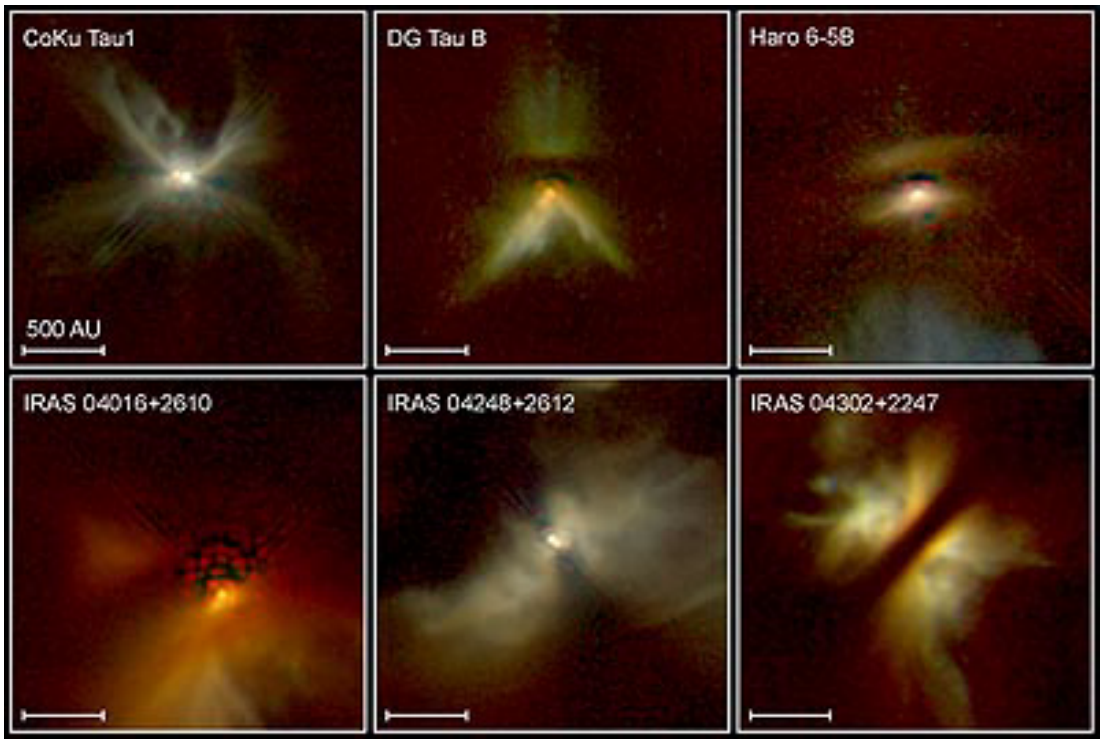

Figure 1 HST-Nicmos images of young stellar disks

NICI will be a powerful tool for probing the in-falling envelopes, disks, and jets of YSOs. Diffraction-limited NIR imaging will resolve structures with scales of about eight AU in the ρ-Ophiuchus and R Coronae Australis molecular clouds, significantly better than that achieved by HST. Past high-resolution studies have selected edge-on YSOs to avoid scattered light problems. With coronagraphic rejection of light from the more pole-on YSOs, we will be able to obtain unbiased surveys of YSOs.

High spatial resolution and low background level will yield unprecedented information on the geometry and distribution of material in infalling envelopes, the geometry and extent of wind-created cavities, and the distribution of material within disks, against which to test YSO models. Virtually no high resolution imaging of YSOs has been performed in the 3-5 micron region where we will obtain ten AU spatial resolutions on deeply embedded structures. High spatial resolution is crucial in order to probe regions ten AU from the stellar surface, where wind/cloud interactions may be revealed. Imaging in spectral lines that probe shocked gas (e.g. [FeII] at 1.64 microns and the 1-0 S(1) line of H_2 at 2.12 microns) will trace the highly collimated jets into the inner regions of accretion disks, perhaps revealing the collimating mechanism. Such observations are fundamental to understanding the role played by outflows in terminating infall, and perhaps determining stellar masses.

Jets contain knots, which are probably created by discrete accretion events from instabilities in the inner accretion disk. At high resolution, these knots will have significant proper motions. By measuring these proper motions, it should be possible to characterize the timescale of accretion instabilities in the disk, and thereby learn much about the physics of the accretion process. An even closer association of T Tauri stars has recently been identified in the vicinity of TW Hydrae (Kastner et al. 1997), which is almost overhead at Gemini South. Given its proximity (55 pc), age (~10^7 yr) and abundance of binary systems, the TW Hya association is ideally suited to studies of diversity and evolution of circumstellar disks.

High-mass (OB) star formation is poorly understood. The formation of massive stars is not merely a scaled-up version of low mass star formation. Massive stars are rarer, disproportionately more luminous, evolve much faster, and are associated with much more violent events than their less massive counterparts, e.g. powerful bipolar jets and outflows, high velocity stellar winds, and supernova explosions. Because of the low probability of forming high mass stars and their extremely short evolutionary timescales (evolving off the main sequence in 10^7 yr) their space density is relatively low. Consequently, the closest massive stars are 450 pc away in the Orion Trapezium cluster. Even at these distances, the picture is complicated by confusion due to multiple sources. Through its high resolution and coronagraphic capability, NICI will be able to conduct high sensitivity searches for outflows and disks in the environs of young O stars and will elucidate formation mechanisms.

2.4 Circumstellar Disks

Circumstellar disks around main sequence stars are the evolved counterparts of disks around YSOs. It is these main sequence circumstellar disks that are the link between planetary system formation and what we know as current, evolved planetary systems like our own. Hence, near infrared coronagraphic studies of these main sequence debris disks will help provide the science link necessary to understand how evolved planetary systems arise, form, evolve and survive.

Main sequence circumstellar debris disks like the IRAS-discovered prototypes Vega and β Pic have been found to be common, occurring around at least 15% of nearby field stars of types A-K. Defining characteristics of these objects include low dust luminosity and optical depth, small gas/dust mass ratio such that dust dynamics are approximately Keplerian, and short dust lifetimes relative to star ages. The dust is clearly “second generation”, i.e. not primordial but released from larger parent bodies such as asteroids or comets. Star age estimates indicate that many of these disks are a few x 10^7 to a few x 10^8 years old, corresponding to the hypothesized time span for construction and heavy bombardment of planets in our solar system.

It is important to point out that second generation material around a star indicates not only the existence of planetesimals, but also of larger masses capable of sending small bodies into fragmenting collisions and star-grazing orbits to release dust and gas. Our solar system (SS) is an example of an old main-sequence (MS) system containing second-generation dust. An external observer detecting the SS dust could thereby infer the existence of remnant planetesimals and their planetary perturbers.

Recent images of some of the famous CS debris systems show them to be disks with central gaps about the size of the planetary region of our solar system, as had been inferred previously. High-resolution imaging has revealed fine structure in some of the disks, offering further indirect evidence of the existence of planet masses. Of the prototype MS CS dust systems, only β Pic so far has detectable dust within the central gap, with model temperatures up to at least 350 K (Fajardo-Acosta et al. 1993). As noted in section II.B.1, the warm grains in that system (Knacke et al.1993) and in the young main sequence system 51 Oph (Fajardo-Acosta et al. 1993) have partially crystalline silicate mineralogy.

Upper limits on the amount of warm dust around other stars (for example Vega, see Aumann et al. 1985) are generally high due to lack of spatial resolution and low contrast of dust flux to stellar photospheres at short IR wavelengths. Ground-based follow-up to IRAS (Aumann and Probst 1991) showed that few MS systems have significant amounts of warm (T > 150K) dust. Several such rare cases have been found and studied recently by Fajardo-Acosta et al. (1998) via mid-IR spectrophotometry. Mid-IR images of HR 4796A (Koerner et al. 1998; Jayawardhana et al. 1998) resolved a central warm dust population radiating at 200-400 K.

The present best photometric sensitivity at 12 and 25 μm to terrestrial-temperature dust around the nearest stars is a few hundred times the optical depth in the SS zodiacal cloud. High spatial resolution will be required for detection of inner-system dust at densities lower than the IRAS/ISO/SIRTF limits of a few hundred "zodis". The nearest stellar system, α Centauri, contains G and K MS stars, and should be an especially interesting target. Unfortunately, it is located at galactic latitude of only -0.7° and is seen against a complex, bright background. This is another situation in which high-resolution coronagraphic imaging by NICI could be employed fruitfully.

The brightness of a 0.3 AU-diameter patch of the SS zodiacal cloud would approximately equal that of Earth at both visual and IR wavelengths. It is estimated that warm dust at more than about 10x SS density would challenge detectability of Earth-like planets via planned space-based mid-IR interferometers like NASA's TPF (Beichman 1998). Since dense exozodi dust may block attempts to detect terrestrial planets around other stars, NICI can play a valuable role as a survey instrument, exploring the frequency of inner-system dust around nearby stars to newly sensitive limits. Ironically, these asymmetries and planetary wakes in dense exozodiacal clouds could themselves be used to infer masses and locations of embedded planets (Dermott et al. 1998).

Circumstellar disks around main sequence stars have been observed from the ground and from space using coronagraphs. The archetype circumstellar disk surrounds Beta Pictoris (Smith and Terrile 1984). Since then, disks around other younger main sequence stars have been imaged, including recent observations of HR4796A and HD141569 from Hubble Space Telescope (Augereau et al. 1999; Schneider et al. 1999, Weinberger et al. 1999). These stars are probably like β Pictoris, and their debris disks represent a middle stage between young protoplanetary disks and old, mature systems. Of particular import are the observations of circumstellar disks around stars with known extra solar planets (Trilling and Brown, 1998; Trilling et al. 2000).

These observed disks are all debris disks - the leftover remains of planetary system formation. In the cases of the stars with known extra solar planets, the debris disks resemble our own Solar System's Kuiper Belt, a ring of debris that surrounds the planets in our Solar System and represents the outer limit of constructive planet formation in the early days of our Solar System. By observing these debris disk remnants of planetary system birth, we learn about how planets form - and, by comparison, how our own Solar System formed.

2.5 Brown Dwarf Observations: Multiplicity and the IMF

Binary star systems do not form in the same way that planetary systems do. Binary stars form from co-collapse of molecular clouds, as opposed to secondary collapse within a circumstellar disk. Thus, studying the multiplicity function of stars reveals information about a formation mechanism different from planetary system formation. Around half of all main sequence stars are in systems of multiplicity (binaries or higher) (Bodenheimer et al. 1993). Naturally, these multiplicities are imprinted signatures of stellar birth environments. However, it is unknown what the multiplicity is for main sequence stars with respect to brown dwarf sub-stellar companions. Additionally, the initial mass function (IMF, Scalo 1986, Meyer et al. 2000) below the edge of the main sequence has only recently begun to be defined, and more data is needed, especially at the lowest masses, to determine where the turnover in the initial mass function is. Thus, to study both the multiplicity of low mass companions as well as the mass function of low mass objects as companions requires the study of faint objects near bright objects, and therefore is an origins-oriented question in which NICI can directly participate.

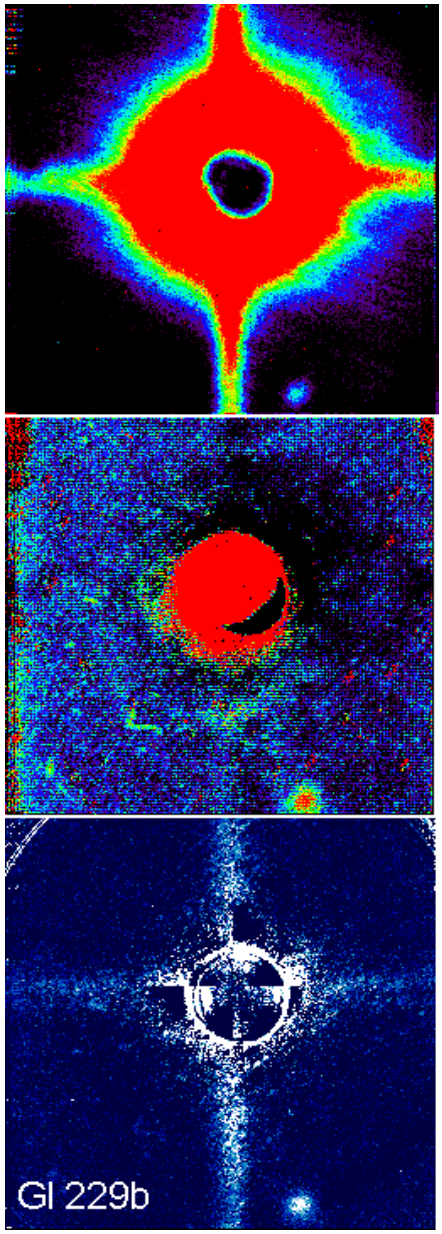

Figure 2-1 GL229B taken at the IRTF with CoCo. The top image is a raw frame, the center is a methane-differenced frame and the lower one is a profile-differenced frame (See NRC Report: Failed Stars and Superplanets, 1998).

Brown dwarfs have been the subject of many papers in the topics of star and planet formation, the dark matter problem, and cosmology. Starting in 1995 (Teide 1, Rebolo et al. 1995; Gl 229 B, Nakajima et al. 1995), found once elusive objects to exist and that they may be numerous in the galaxy. This has raised many questions about their atmospheres, activity, weather, internal structure, evolution, and the sub-stellar Initial Mass Function (SIMF). The numbers of high mass BDs (75 to 40MJ) found in the field and in young open clusters and associations indicate that the IMF does not have a turnover at the sub-stellar limit (Martín et al. 1997a; Reid et al. 1999). However, theoretical models of star formation (e.g., Bodenheimer et al. 1993) have predicted that there has to be a minimum mass for fragmentation (e.g., Scalo 1988), which should imply a cutoff of the IMF below a certain mass. Such a minimum mass is very uncertain. Estimates have been made since the early 1970s, and they vary by two orders of magnitude from one tenth of a solar mass to about 1MJ. The fact that many field BDs have already been found effectively rules out minimum masses above the sub-stellar limit. An observational determination of the turnoff of the IMF will be a critical constraint for general models of star formation. If the SIMF extends to very low masses (~1MJ), this will significantly impact our understanding of giant planet formation. There will be two evolutionary paths, with distinctly different initial conditions, leading to essentially identical objects.

The first unambiguous detections of sub stellar low mass (brown dwarf) companions have only recently been made. The brown dwarf Gl229B was discovered (Nakajima et al. 1995) by direct imaging with a coronagraph working in visible light and follow up studies (c.f., Oppenheimer et al. 2000) have also been carried out with similar instruments. The cool spectrum of GL229B made visible detection relatively difficult from the point of view of high relative background levels. Follow up observations at the IRTF show that the object is relatively easily detected and its light easily isolated in the near infrared (Figure 2-2) by use of the cryogenic coronagraphic relay, CoCo (Wang et al 1994). Additionally, the study of stellar multiplicity can be extended to companions to sub stellar objects. Recently, Martín et al. (1999), Koerner et al. (1999), Basri and Martín (1999), Martín et al. (1998), among others, have found that the frequency of binarity in sub stellar objects may also be high. Martín

et al. (2000) have found, using the adaptive optics system at the Keck telescope, that the Gl569 system has a very low mass companion binary (Gl569B and C) to the cool M star Gl569A, thus demonstrating that companions and multiplicity can be two sides of the same coin.

Low-mass BDs are incredibly faint and thus difficult to find, but younger ones are easier to see. Our best chance of finding low-mass BDs as companions is to search for them in young clusters and associations, or as companions to young stars, or even as companions to young BDs. (Note also that the radial velocity surveys do not study young active stars, so the multiplicity and number of companions to young stars is quite unknown.) Recently, an L dwarf has been identified in the young (~ 5My) open cluster Σ Ori (Zapatero-Osorio et al. 1999). Using recent evolutionary models that have been tested against the BD sequence of the Pleiades (Chabrier et al. 2000), a mass of order 15MJ was derived for it. If the SIMF of Σ Ori is typical of the Galactic disk, BDs exist down to at least 15 MJ, with an IMF slope rising at decreasing masses. The Deuterium-burning mass limit is at $13M_J$, so we are very close to crossing it in Σ Ori.

Radial velocity surveys have found a Brown Dwarf "Desert", i.e., an absence of BD companions to G and K-dwarf primaries within ~5AU (Marcy et al., 2000). On the other hand, BD companions to BD primaries appear to be relatively common. We know of the existence of one double-lined spectroscopic binary with BD components in the Pleiades (Basri and Martín 1999); and four binaries in the field where both components are ultra-cool dwarfs (Martín et al. 1999b, 2000a; Koerner et al. 1999). All of them have separations less than 10AU. The separation distribution of G and K dwarfs in the solar vicinity has a broad peak between 5 and 40 AU (Duquennoy and Mayor 1991). The mean orbital period is 180 years. However, BDs seem to prefer smaller separations. It is possible that planets around BDs also tend to be closer than planets around stars. There appears to be no prohibition against the formation of a small-scale solar system around BDs. The implication is that high angular resolution is extremely important for imaging planets around BD primaries.

The properties of BDs are so different from those of stars, that two new spectral classes have been proposed for them. The L class is cooler than M. It is characterized by the decrease in TiO and VO bands due to metal condensation in dust grains, and the presence of strong resonance lines of alkali elements (Martín et al. 1997b, 1999; Kirkpatrick et al. 1999). The prototype of this class is GD165B (Becklin and Zuckerman 1988). A second spectral class, either T (Kirkpatrick et al. 1999) or H (Martín et al., 1999) has been proposed for even cooler dwarfs. This class is characterized by the presence of strong methane bands in the near-infrared spectrum. The benchmark of this class is Gl229B (Oppenheimer et al. 1995).

The study of brown dwarfs to determine the multiplicity and mass function is obviously a difficult one, compounded by the relative faintness of the companions and proximity to their primaries. This project will require all of the capabilities of NICI. The low luminosity of brown dwarfs will clearly require the eight-meter telescope of Gemini, as well as the adaptive optics capabilities of NICI, in order to detect these faint objects. The high dynamic range will require the optimized coronagraph and the proximity of low mass companions to their primaries will require the high resolution imaging. NICI's dual channel capability will be an effective tool to identify brown dwarfs spectrally. As discussed above, the lowest mass brown dwarfs have spectral features not found in other stars and sub stellar objects.

Simultaneous imaging in and out of a low mass companion-specific filter, which takes advantage of the spectral signature of these lowest mass objects, will cause these methane-rich objects to stand out sharply in contrasted, subtracted images. We image the field in both broadband and narrow-band filters. Objects that absorb methane, for example, appear in only the broadband image. Thus, the subtracted image will show only the coolest objects, since objects without methane in their atmospheres will appear in both filter images, and thus subtract out. Only the cool low mass companions will remain in the image.

NICI will be able to carry out a deep companion search to a delta magnitude of at least 14 within 0.5 arcsec, thus revealing sub stellar companions (which might typically have delta magnitudes of 5-15 at K band (Burrows et al. 1997)). NICI, optimized for AO and with the added benefit of a customized coronagraph, should be an ideal instrument for advances in the fields of sub stellar companions and multiplicity. Critical data needed to help constrain the slope of the IMF as well as the multiplicity function below ~0.3 Msun can come from studies of faint stellar and sub stellar companions. With NICI, we will be able to detect companion objects in the range 0.01-0.1 Msun Brown Dwarfs.

2.6 The Search for Extra solar Planets

The direct imaging of extra solar planets is, in many ways, the defining circumstellar imaging problem. There have been many suggestions and claims as to how it should be done, with what instrumentation, at what wavelength etc. The one area of general agreement, however, is that it is very difficult. The problem is, in fact, an extremely complex one that involves both optical imaging properties of the telescope and the physical properties of the planets themselves. We draw on both to present the basic detection considerations. The factors involved in this kind of detection are discussed in some detail because they capture the essence of coronagraphic observing, and illustrate much of the thinking that went into the design of the instrument.

In general, planetary spectra are determined by the reflected light from the stellar primary, as modified by the planetary atmosphere and thermal emission from the cooler planet. Which component dominates obviously depends on the planet, the primary, and the wavelength of observation. Searching in reflected light, one looks for the brightest stars to get the most photons. In thermal emission, we look for the lowest luminosity primaries to minimize the contrast between the star and the planet. We will look, therefore, at planet detection in two contexts: a search in reflected light of the brightest, closest, normal stellar population, and a search in thermal emission for planets around the lowest luminosity objects, particularly brown dwarfs.

Throughout most of the visible spectral region, the spectra of Jovian planets are close to those of the stars they orbit, with some relatively narrow absorption lines arising from the planetary atmosphere. Starting shortward of the near infrared, the reflection spectrum is modified by the planetary molecular composition, with broad absorption features due primarily to methane, and by the increasing thermal emission from the planet. In Figure 2 we show some of the evolutionary models for planetary flux density for $5M_J$ planet. The models show that for the thermal component, spectral emission in the near infrared can vary by orders of magnitude with the age and the mass of the planet. Even for normal stars, it is possible in younger systems for the thermal emission to be comparable to the reflected light in the near infrared. In general, the thermal emission peaks for younger and for more massive planets. The latter is important because planet non-detections in thermal emission must be considered as constraints in the age-mass plane.

Through the mid-infrared, the intrinsic thermal emission of the planet generally dominates. This more favorable star-to-planet balance near ten microns has led many researchers to conclude that this is the optimal planet detection wavelength. However there are many more wavelength dependent factors that must be taken into account. The image area over which we collect background increases like λ^2 but the image Strehl factor also increases like $s_1^{\frac{1}{\lambda^2}}$ where s_1 is the Strehl factor at a wavelength of 1μm and λ is the wavelength in microns.

The background against which the planet must be detected is the sum of the residual stellar scattered light and the combined sky and telescope background. These background sources must be combined in order to estimate the quantum noise in the detection. Shot noise estimates do not really characterize the difficulty of making this observation because they ignore the systematic aspects of removing the large background in order to get to the quantum noise limit (Brown and Burrows, 1987, Ftaclas, 1992, 1995, Walker et al. 1994). Shot noise estimates give minimum integration times, but it is possible to do considerably worse. Furthermore, no matter how long the estimated integration time is, one could, in principle, just integrate that long. But if the background cannot be removed, the observation cannot be made at all. Experience has shown that the ability to make this subtraction is not at all dependent on the shot noise in the image as long as quantum considerations are satisfied. Handling of the background has been the focus of planet detection for some time.

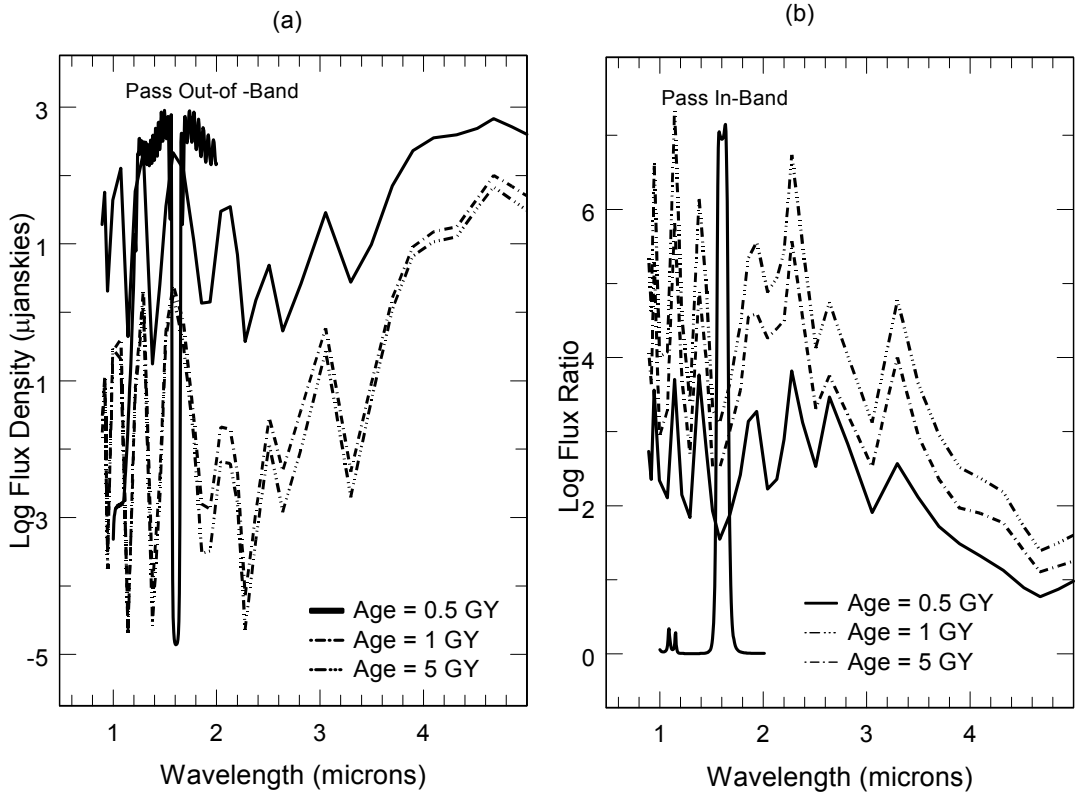

Figure 2 (a) Evolutionary models for a 5 M_J Planet and (b) The ratio of the flux ratio for a 50 M_J brown dwarf to that of the planet at the same age. In both plots we have added complementary filter designs meant to isolate the 1.6 micron methane feature.

The sky/telescope background is essentially independent of short-term fluctuations in the seeing record, and can be accurately estimated with frequent beamswitching with small re-pointings of the telescope. The residual scattered light, however, is critically dependent on the detailed turbulence record, and the large pointing changes usually required to find a star of comparable brightness limit repeatability (Terrile 1995, Kalas and Jewett 1996). This occurs even in space observations. Krist et al. (1998) report that in working with NIC images in a search for faint companions, the best they could do with frame differencing was a background reduction to one part in fifteen, and only outside a radius 1.75 arc seconds. Inside this radius, the residuals were significantly larger.

For the Gemini telescopes, the wings of the stellar PSF within a few arc seconds of the star are dominated by the effects of atmospheric turbulence. On average, the scattered intensity will be given by $I_s(\lambda) \propto \frac{1}{\lambda^4} PSD\left(\frac{\theta}{\lambda}\right)$ where $PSD(f)$ is the turbulent power spectrum at spatial frequency f, and θ is the field angle in the focal plane. Again, the leading, strong wavelength dependence has always suggested working at longer wavelengths where the scatter seeks to be lower. The Kolmogorov power spectrum is of the form $PSD(f) \propto f^{-\frac{11}{3}}$ (note that the wavelength dependence of the Fried length is already included in the factor of λ^{-4}). When $f = \frac{\theta}{\lambda}$ is substituted, we get $I_s(\lambda) \propto \lambda^{-\frac{1}{3}}$. Since the scattered light must be collected over the planet Airy disk whose area increases like λ^2, it follows that the scattered light collected per Airy disk will scale like $\lambda^{\frac{5}{3}}$. In other words, as far as scattered light is concerned, the steep atmospheric power spectrum and growing Airy disk size erode the advantage to going to longer wavelengths. This remains true until a significant improvement in the relative brightness of the planet occurs in the thermal infrared. One must

also deal with the steep increase in sky and telescope thermal emission at longer wavelengths. For ground-based, scatter dominated imaging of a solar twin system at 5pc, typical values for the ratio of planet peak surface brightness to local background surface brightness are of order 10^{-3} – 10^{-4} in reflected light at 1-2 microns and, of course, can get significantly worse as the apparent angle between the star and the planet decrease. Since the scattered intensity is falling off like $\theta^{-\frac{11}{3}}$, but the reflected light intensity is only falling off like θ^{-2}, it follows that direct imaging is more sensitive to planets at larger orbital radii.

Assuming a planet orbital radius sufficiently large that thermal input from the star is not an issue, then as the stellar luminosity drops, the reflected light component decreases but the thermal emission remains constant. Therefore, the contrast ratio between the star and the planet grows more favorable for intrinsically fainter stars even without going to the mid infrared. The natural conclusion of this argument is to look for planets around brown dwarfs. In the discussions of Section 2.5, we note that the expectation is that by the time NICI is in service, a significant population of nearby BDs will be identified, so we consider planet detection by thermal emission. There are several compelling scientific drivers for this search apart from those that motivate any planet search. Any companion to a BD is intrinsically of interest, and searching for planets is a natural extension of a faint companion search aimed at determining multiplicity in the BD population. Second, detection of any planet around a BD would determine the mass of the BD, and possibly its age.

In Figure 2 we have plotted the ratio of the spectral flux from a 5 M_J planet to that from a 50 M_J BD, again using the models of Burrows et al. Looking only at the minima in these plots (the best places to look for planets) we note that the flux ratio varies only from about 10^2 - 10^5. This is a significant improvement over the value of 10^9, the canonical value for Jovian planets seen in reflected light, and it is achieved in the near infrared. From a background removal point of view, this would be a relatively easy observation for NICI. The difficulty lies in the absolute flux levels. One μJansky is a flux of order $750/\lambda_\mu$ photons s^{-1} μm^{-1} received by the Gemini collecting area (λ_μ is the wavelength in microns). At 1.6 μm this gives a count rate of 470 photons s^{-1} μm^{-1}. The estimated background count at that wavelength is 1.6×10^6 photons s^{-1} μm^{-1} arcsec^2. Because of the AO system, the image core at that wavelength is only about 0.04 arcsec wide (FWHM) or just over two NICI pixels wide. The total background count in four NICI pixels would then be 2000 photons s^{-1} μm^{-1} or four times the image counts. Not all the photons collected from the planet end up in the image core, but even allowing for only ten percent in the core, the observation does not look unreasonable. The problem, of course, is that for background dominated observations, the integration time scales inversely with the square of the planet flux. Going down to flux densities of 0.1 to 0.01 μJy, more typical of older or less massive planets, the integration times can get quite long. This case nicely illustrates the value of adaptive optics in background-limited observations, and it is the key to making observations like this.

One important aspect of looking for any companions to BDs is that the ages of all components of the system are constrained to be identical. This is not usually a consideration for reflected light searches, but it is a significant factor for BDs. For example in Figure 2 the flux ratio at 1.6 μm is about one order of magnitude better than it is at 2μm for an evolved system at 5GY. But it is two orders of magnitude better for the system at an age of 1GY. By determining the flux ratio in different bandpasses, it should be possible, in combination with the evolutionary models, to place bounds on the system age.

Faint objects like brown dwarfs are usually thought of as the object of coronagraphic searches, as opposed to coronagraphic targets. All unresolved sources, however, produce an identical PSF with extended wings. It is more obvious in bright sources, but still there in fainter ones. For BD observations, it is likely that the combined sky and telescope backgrounds will dominate the stellar PSF wings, so NICI will, in all likelihood, not improve the integration time for these observations as it does for bright stars. Once the sky and telescope contributions are removed by beamswitching, however, we are left with an image dominated by the sidelobes of the BD and NICI will reduce that. It is useful to recall that the BD, planet, and background light all go through the telescope as independent (i.e. incoherent), simultaneous experiments.

There are two basic approaches to detecting a planet in a background-dominated image: differencing and filtering. In the former, the image is compared to a reference image in which the planet is not presumed to be present. In the latter, the planet image is detected because it differs in spatial characteristics from its surroundings. If the background were extremely smooth, for example, it would be easy to pick out the steep sides of the planet image core digitally, as long as shot noise considerations allow it to be detected. An

example of this kind of filter (Ftaclas et al. 1994) is shown in Figure 3. It depends on the fact that that the effect of bandwidth is to smear speckles radially. The scatter sidelobes are sampled along a radius on either side of the pixel location. These samples are used to generate an estimate of the background at the pixel location, which is then subtracted out, as in high pass filtering. A gap the size of the image core at the pixel prevents contamination of the estimate by the planet signal.

The level of the post-filtered background depends critically on the spatial quality of the input background. For the case illustrated, the RMS residual was about ½% of the input. The input was a broadband fixed speckle pattern, so there was no temporal smoothing. One important conclusion from this study was that the post-filter noise level was found to be roughly proportional to the pre-filter input. When noise scales with the background rather than the root of the background, longer integration does not improve the signal to noise ratio. This underscores the assertion that it is background removal that drives the observation, not shot noise.

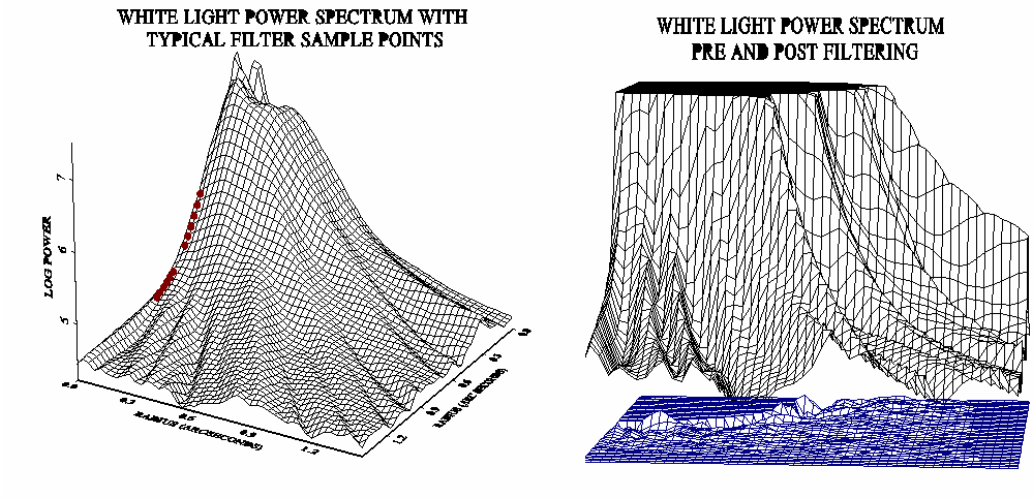

Figure 3 A digital filter designed to look for point sources. The log scaled background and sample points are shown on the left. The background (linear scale) and post-filtered residuals are shown on the right.

As noted above, frame differencing has not been particularly effective because of the need to use two different stars. Frame differencing to better than 1% (Trilling and Brown, 1998) is being done at the IRTF using CoCo by imaging in and out of the methane band near K. This approach is very effective because the telescope never moves off the star, and because the switching can be done relatively quickly to track changes in seeing. Combining these very promising results at the IRTF with the argument that atmospheric turbulence does not repeat (Racine et al. 1999), has led us to consider a dual beam configuration. The goal is to make differential measurements rather than be forced into making absolute comparisons of measurements made hours or days apart.

2.7 Science in Support of NASA Missions

In addition to its charter mission to investigate the birth and evolution of stars and planetary systems, NICI will play a major role in support of other NASA initiatives. As with the IRTF, Keck, and other NASA support facilities, valuable preparatory, follow-up and interpretive work can be done with coronagraphic imaging.

2.7.1 Coronagraphs and Astrometry: (SIM)

There has always been a close connection between coronagraphs and astrometry. Figure 4 is an image of Procyon made at the IRTF with the CoCo coronagraphic relay. It was one of the very first images ever taken with the instrument, and was part of a program to image known binaries with large magnitude differences. It turned out to be the first time Procyon and its white dwarf companion had ever been imaged simultaneously. A careful measurement of their angular separation resulted in a new orbit for the pair, and consequently a new mass determination for Procyon (Girard et al. 2000).

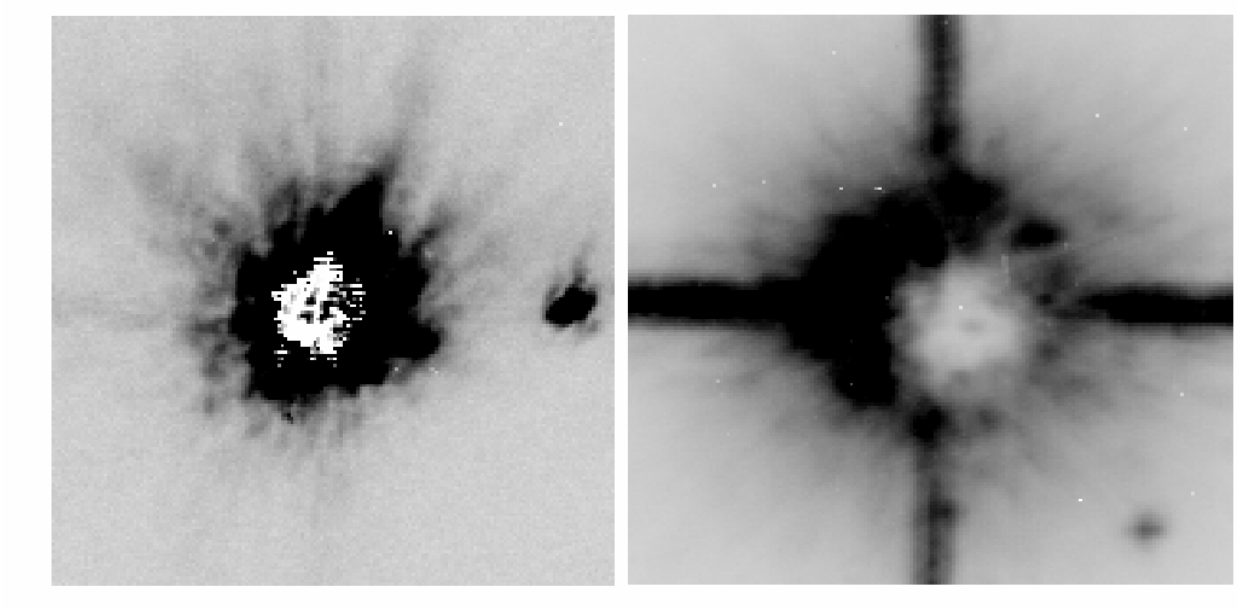

Figure 4 Images of Procyon taken at the IRTF with (right) and without (left) CoCo. The white dwarf Procyon b is visible in the lower right hand corner of the right and not visible on the left. Spot at right in left image is a ghost.

When a faint companion is detected for relatively nearby stars, the next step would be a follow-up image separated in time. This serves the two-fold purpose of verifying the common distance by common proper motion and the beginning of the determination of the orbit. Thus, starting with the image, we move to astrometry for verification and analysis. This relation is purely symmetric. Astrometric observations utilize circumstellar imaging for verification and analysis.

The Space Interferometry Mission (SIM) will be launched in 2006 with a goal of producing high accuracy (4 microarcsec) astrometric measurements on stars as faint as 20th visual magnitude with eight-hour integrations. Depending on the beam combination geometries implemented, it could have some imaging capability, and perhaps a nulling capability for reducing the brightness of a central star to investigate its surroundings. Its goal astrometric precision will be reached over its five-year mission by virtue of repeated measurements made against an astrometric reference grid known to one microarcsec accuracy.

SIM has a rich and varied science program, but the dominant themes are critical distance scale measurements and the search for low mass companions down to Earth-mass objects. There are several symbiotic connections between NICI and SIM. The nature of the grid stars is crucial to SIM performance since there is no other astrometric catalog at that level of precision. Since SIM only measures the centroid of the received light from a star, it interprets all shifts in this centroid as motion of the star. Complex stellar environments can easily produce significant centroid shifts without any real motion of the star. NICI can provide deep imaging of the circumstellar environments of grid stars. It can help evaluate candidate grid stars prior to launch and help resolve anomalies after launch.

Astrometric signals from nearby stars indicating the possibility of low mass companions can be followed up on the ground with NICI. The time scale of the SIM mission is comparable to the periods of inner Solar System planets, but shorter than outer planet orbital periods. Thus, SIM will detect suggestions of long-term, non-linear drifts (as did Hiparcos), but not be able to get complete orbital solutions. With NICI's greater sensitivity to outer planets, it would be possible for a fairly complete search and definition of the closest systems.

2.7.2 Future IR Imaging Missions SIRTF, SOFIA, NGST

After decades of discussion within the community on an infrared capability in space, it appears that NASA has embarked on an ambitious program to create a suite of IR instruments with powerful capabilities. SOFIA, SIRTF and NGST are in various stages of planning, but are all scheduled to come on line in the time frame NICI will be operating. In Table 2-1, we summarize each of these missions with comparable data for NICI. We outline each of these programs below:

The **Stratospheric Observatory for Infrared Astronomy (SOFIA)** will replace the aging Kuiper Airborne Observatory with a 2.5m aperture telescope mounted in a converted jet transport. It will fly over a larger fraction of the water vapor in the Earth's atmosphere than ground-based installations, and image in regions of the spectrum closed to ground-based facilities. Although it escapes much of the atmospheric water vapor, it is subject to enhanced turbulence due to the motion of the plane.

The **Space Infrared Telescope Facility (SIRTF)** will be an 84cm aperture, cryogenically cooled, all Beryllium telescope capable of diffraction limited imaging into the far infrared. It will be in an orbit about the Sun, trailing further away from the Earth as time goes on. Its mission is limited to 2.5 years (with a goal of 5 years) by the lifetime of its liquid Helium supply. SIRTF is designed around its long wave sensitivity and diffraction limited capability. The telescope is not expected to be diffraction limited below six microns.

The **Next Generation Space Telescope (NGST),** scheduled for launch in 2009, is currently under aggressive study. It will be a passively cooled, eight-meter aperture telescope in orbit at L2 that will utilize many innovative telescope technologies to control cost and weight. It represents a significant IR capability in space, but in order to deliver an aperture that large to orbit, it will have a segmented aperture and self-erect on-orbit. Segmentation produces a pupil function that is considerably more complex than Gemini's and less favorable for coronagraphic work. The current baseline instrument suite projected for NGST is primarily oriented towards wide-field imaging and spectroscopic modes. Although free of absorption due to the Earth's atmosphere, it is not free of phase perturbations due to its segmented aperture and ultra-lightweight optics, so it is not expected be diffraction limited shortward of 2 microns.

NGST will be able to image in windows where the atmosphere is opaque with a comparable aperture to Gemini, but NICI will still provide valuable services to the project. NICI is a perfect high-resolution follow-up instrument to complement NGST's survey capability. More importantly, as we have indicated throughout this discussion, the defining line between what can be accomplished on the ground and what needs to be done in space has grown steadily less clear. With the very high cost factors associated with almost any space operations, state-of-the-art instruments like NICI will be well positioned to answer significant questions about ground-based near IR imaging, and to provide valuable guidance for final instrumentation, configuration, and tolerancing decisions for NGST.

	SIRTF	SOFIA	NGST	Gemini/NICI
Aperture	0.9m	3.0m	8m	8m
Operating Wavelength	3 -180μm	0.3–600μm	0.6 - 30μm	1-5μm
Diffraction limited wavelength	6.5μm	1 – 5μm	2.0μm	1μm
Minimum Pixel Scale	1.2"	0.12"	0.029"	0.018"
Projected Date of Service	Dec. 2001	Fall, 2002	2009	2004
Platform Type	Solar Trailing Orbit	Air-borne	Space, L2	Ground

Table 2-1 NASA Infrared Capability Over the Next Decade

Looking at the entries Table 2-1, we can see that the total capability is significant and that there are both common areas and significant differences in these facilities. It is easy to imagine a fertile interchange between all of these facilities. We would expect that not only will NICI support observations made with these facilities, it will also benefit from them. Clearly there is a follow-up role for NICI, just as ground based imaging was used to follow up the IRAS detection of excess emission from Beta Pictoris. In this group of instruments, NICI's role of high-resolution deep circumstellar imaging appears to be unique and valuable.

2.7.3 Future Planet Searches

The great difficulty of imaging a planet of any variety has led to a near term focus on Jovian planets because of their larger size and assumed larger angular separations compared to Terrestrial planets. The ultimate goal of the Origins program, however, is the detection and characterization of earth-like planets. To implement this plan, NASA has begun study of a large-scale, interferometric array, the Terrestrial Planet Finder (TPF). The objective is to use a nulling configuration to eliminate the light of the central star, and rotational modulation of the interferometer's fringe pattern to detect planets. Working in the 5 to 10 micron region, it will have a coarse spectral capability with enough spectral resolution to detect the broad spectral features associated with methane, water, Carbon Dioxide and Oxygen. Simulations of the system show that for nearby stars, Earthlike planets could be detected in hours to days, and characterized in tens of days.

The gain of a more favorable star-to-planet ratio at ten microns, however, brings with it some troubling complications for detection. There is the background signal created by the zodiacal emission of our own solar system. This can be overcome by a combination of large apertures and spacecraft orbits close to that of Jupiter. A much less well-understood concern, however, is the effect of a zodiacal cloud in the solar system under observation. Optically, such a cloud would be unresolved in the sub-aperture of the interferometer so that, in effect, the total light of the cloud would appear as background to the planet. For the case of the solar system, that implies a signal from the dust 10^4 times brighter than the signal from the Earth. Moreover, the motion of planets through the zodiacal dust sweeps out lanes in the dust and results in density enhancements of order 10% leading and trailing the planet.

We have good reason to expect that zodiacal dust clouds, where they exist, would cause a bright and structured background for planet detection. The frequency and expected brightness of expected exozodiacal clouds is only weakly constrained by current observations. Models of planet formation show that in only about half the cases does an asteroid belt form which could provide a source of zodiacal dust. Therefore, it is possible that dust will not be a problem in many cases. Arguments based on other observations, however, have concluded that our zodiacal cloud has atypically low density. Given the scale of the TPF mission, it would be risky to fly it without some understanding of the target population. NICI could set upper limits on zodiacal emission, and by imaging very close to primaries, could develop secondary information as to the extent of planet forming activity.

2.8 References

Adams, F.C., Lada, C.J., & Shu, F.H. 1987, *ApJ* 312, 788.

Augereau, J.C., Lagrange, A.M., Mouillet, D., and Ménard, F. 1999

Aumann, H.H. 1985, *ASP* 97, 885-891.

Aumann, H.H., Probst, R.J. 1991, *ApJ* 368, 264-271.

Basri and Martín 1999, *AJ* 118, 2460.

Becklin, E.E., and Zuckerman, B. 1988, *Nature* 336, 656-658.

Beichman, C.A. 1998, *SPIE* 3350, 719-723.

Bodenheimer, P., Ruzmajkina, T., and Mathieu, R.D. 1993, Protostars and Planets IV, 367-404.

Brown, R.A. and Burrows, C.J. 1987, *Icarus* 87, 484-497.

Burke, B.F. 1992, NASA, Solar System Exploration Division Report.

Burrows, C.J., Stapelfeldt, K.R., Watson, A.M. et al. 1996, *ApJ* 473, 437.

Burrows, A., Marley, M., Hubbard, W.B., Lunine, J.I., Guillot, T., Saumon, D., Freedman, R., Sudarsky, D., Sharp, C. 1997, *ApJ* 491, 856.

Chabrier, G. et al. 2000, *ApJ*, submitted.

Close, L.M., Roddier F., Northcott, M., Roddier, C. & Graves, J.E. 1997, *ApJ* 478, 766.

Dermott, S.F., Grogan, K., Holmes, E.K., and Wyatt, M.C. 1998, Exozodiacal Dust Workshop, 59.

Duquennoy & Mayor 1991, *A&A* 248, 485.

Elachi, C. et al. 1996, A Road Map for the Exploration of Neighboring Planetary Systems, JPL Technical Report.

Fajardo-Acosta, S.B., Telesco, C.M., and Knacke, R.F. 1993, *ApJ*, in press.

Fajardo-Acosta, S.B., Telasco, C.M., and Knacke, R.F. 1998, *AJ* 115, 2101-2121.

Ftaclas, C., et al. 1992, HDOS Project –Final Report, PRB110348.

Ftaclas, C. 1995, Proceedings of the Fifteenth National Solar Observatory/Sacramento Peak Summer Workshop, ed. Kuhn, J.R. and Penn, M.J., 1987, (World Scientific, Singapore) 181.

Girard 2000, *AJ*, in press.

Hartmann et al. 1993, Protostars and Protoplanets III.

Jayawardhana, R., Fisher, S., Hartmann, L, Telesco, C., Pina, R., and Fazio, G. 1998, *ApJ* 503, L79.

Kalas, P. and Jewitt, D. 1996, *Astronomical Journal* 111, 1347.

Kastner, J.H., Zuckerman, B., Weitraub, D.A. and Forveille, T. 1997, *Science* 277, 67.

KenKnight, C.E. 1977, *Icarus* 30, 422.

Kirkpatrick, D. et al. 1999, *ApJ* 519, 834.

Knacke, R.F., Fajardo-Acosta S.B., Telesco, C.M., Hackwell, J.A., Lynch, D.K., and Russell, R.W. 1993, *ApJ* 418, 440K.

Koerner, D.W., Ressler, M.E., Werner, M.W., and Backman, D.E. 1998, *ApJ* 503, L83

Koerner, D.W., Kirkpatrick, D., McElwain, M.W., and Bonaventura, N. 1999, *ApJ* 526, L25-L28.

Krist, J.E., Golimowski, D.A., Schroeder, D.J., and Henry, T.J. 1998, *Publications of the Astronomical Society of the Pacific* 110, 1046-1058.

Levy and Lunine, eds., Univ. of Arizona Press, Tucson.

Mannings et al. eds., Univ. Arizona Press, Tucson.

Marcy, G.W., Cochran, W.D., and Mayor, M. 2000, Protostars & Planets IV, ed. V. Mannings, A.P. Boss & S.S. Russell (Tucson: University of Arizona Press), in press.

Marois, C, Doyon, R., Racine, and Nadeau, D., 2000, *PASP* 112, 91.

Martín, E.L., Zapatero Osorio, M. R., & Rebolo, R. 1997a, ``Brown Dwarfs and Extra solar Planets", ASP Conf. Series 134, p. 507.

Martín, E.L. et al. 1997b, *A&A* 327, L29-L32.

Martín et al. 1998, *ApJ* 509, L113-L116.

Martín, E.L., Basri, G., Brandner W. 1999a, *Science* 283, 1718.

Martín, E.L. et al. 1999b, *AJ* 118, 2466.

Martín, E.L. et al. 2000, *ApJ* 529, L37-L40.

Meyer et al. 2000, Protostars and Planets IV, ed. V. Mannings, A.P. Boss & S.S. Russell (Tucson: University of Arizona Press), in press.

Nakajima, T. et al. 1995, *Nature* **378**, 463.

O'dell et al. 1993, *ApJ* **410**, 696.

Oppenheimer, B. et al. 1995, *Science* **270**, 1478.

Oppenheimer et al. 2000, in Protostars and Planets IV, ed. V. Mannings, A.P. Boss & S.S.

Russell (Tucson: University of Arizona Press), in press.

Padgett, D.L., Brandner, W., Stapelfeldt, K.R., Strom, S.E., Terebey, S. and Koerner, D. 1999, AJ 117, 1490.

Racine, R., Walker, G.A.H., Nadeau, D., and Doyon, R. and Marois,C 1999, PASP 111, 587.

Rebolo, R., Zapatero Osorio, M. R. and Marti n, E. L. 1995, Nature 377, 129.

Rebolo, R., Zapatero Osorio, M. R. and Marti n, E. L. 1995, Nature 377, 129.

Reid et al. 1999, ApJ 521, 613.

Scalo, J.M. 1986, Fundamentals of Cosmic Physics 11, 1-278.

Scalo, J.M. 1988, Molecular Clouds/Milky-Way & External Galaxies, 201.

Schneider, G., Smith, B.A., Becklin, E.E., and Koerner, D. 1999, ApJ 513L, 127S.

Smith and Terrile 1984, Science 226, 1421.

Spitzer, L. Jr. 1978, American Scientist 66, 426.

Terrile, R.J. 1995, Private communication.

Trilling, D.E., and Brown, R.H. 1998, Nature 395, 775-777.

Trilling et al. 2000, ApJ, in press.

Walker, G. A., Walker, H., Walker, A., Racine, R., Fletcher, J.M., and Mclure, R.D. 1994, PASP 106, 356

Wang, S., Toomey, D.W., Brown, R.H., Cavedoni, C.P.,. Hua,, R., Stahlberger, W.E., Owensby, P. and Ftaclas, C. 1994, SPIE 2198, 578 (1994).

Weinberger, A.J., Becklin, E.E., Schneider, G., Smith, B.A., Lowrance, P.J., Silverstone, M.D., Zuckerman, B., and Terrile, R.J. 1999, ApJ 525, L53-L56.

Zapatero-Osorio, M. R. et al. 1999, ApJ 524, L115.

2.9 Science Channel Performance

Quantifying the performance of NICI is a much broader question than when describing a traditional imaging camera. The performance is described here in two ways. The first is a limiting magnitude when NICI is used as a traditional imaging camera. This is measured on the telescope. These limiting magnitudes are listed in the table below. Gemini will supply an observing tool for NICI that will allow calculation of performance data for NICI. The table supplied here gives a rough overview of the NICI performance.

NICI Traditional Performance (3 sigma in 1 hour)

Filter	J	H	K	L	M
3 sigma 1 hour	TBM	TBM	TBM	TBM	TBM

Coronagraphic Performance

Of greater interest for NICI is the performance in its core science mode which is coronagraphic differential imaging of methane absorbing objects around nearby stars. This is a function of the primary star brightness and the separation. The most useful way to represent this data is a graph of the contrast versus separation. A very conservative model produced the graph below. This will be replaced with a measured version once the instrument is at the telescope.

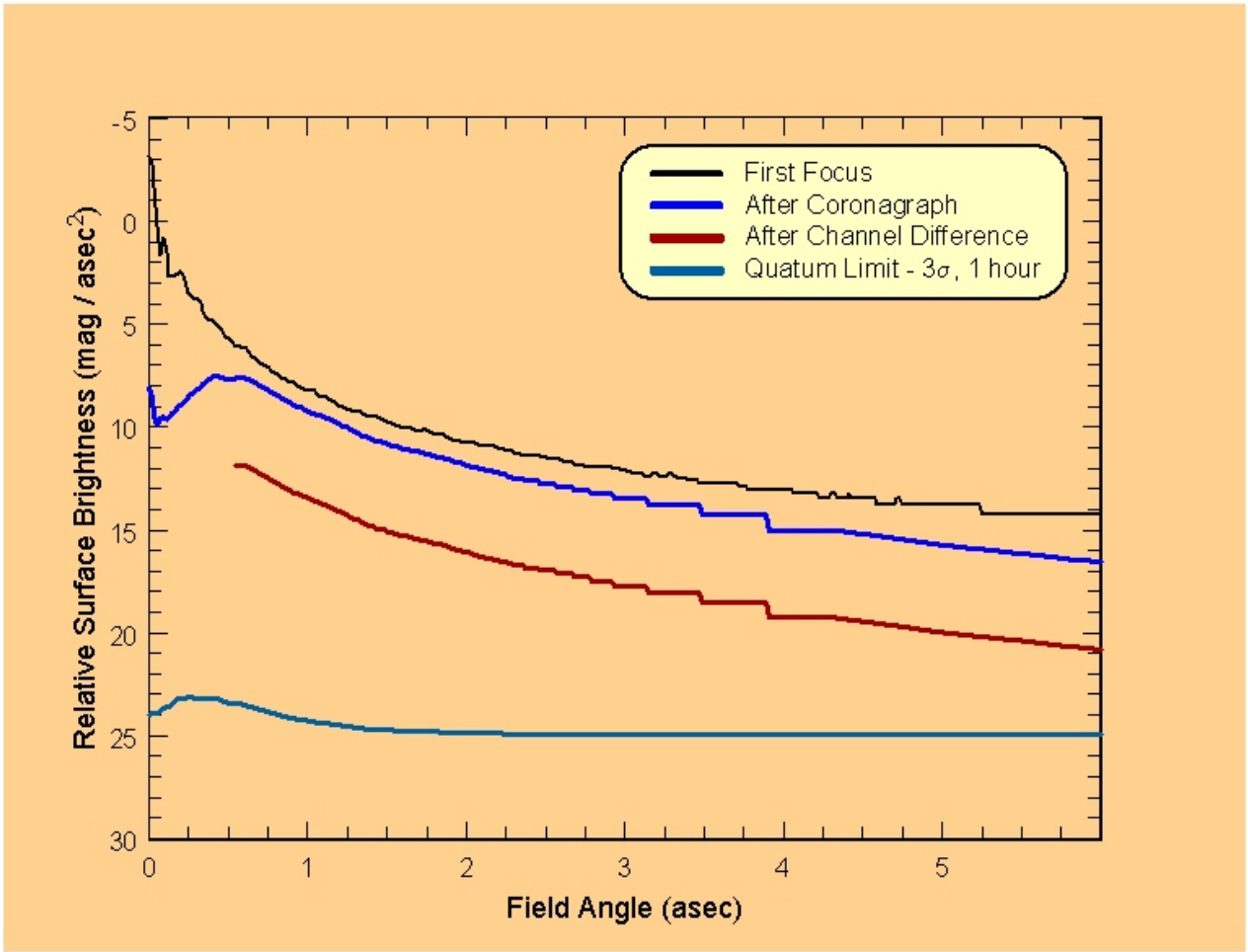

2.10 AO Performance

The adaptive optics portion of the NICI instrument is crucial for achieving the required sensitivities. For very high quality imaging systems the term “Strehl ratio” is the best way to describe the imaging performance. The Strehl ratio is the ratio of the intensity at the center of the diffraction image formed by an aberrated optical system to the intensity when an aberration-free system is used. The measured Strehl ratios for the NICI system are listed in the table below.

AO Performance - Strehl Ratio versus Wavelength

Filter	J	H	H (1%)	K	L	M
Strehl Ratio	TBM	TBM	TBM	TBM	TBM	TBM

3 Instrument Overview

NICI is a dual science channel instrument with integrated adaptive optics aimed at high resolution frame differencing optimized for observations of faint objects in the immediate vicinity of bright sources. NICI is a coronagraphic imager with a wavelength range of 1 - 5 μm.

The key instrument elements are:

- Dual channel camera. This camera is the “heart” of the instrument. By making simultaneous, dual beam differential observations, we will reach new levels in background removal.
- Dual 1024x1024 InSb Detectors. One detector per channel operating over the 1-5 micron with range with high density sampling at 0.018 arcsec/pixel.
- Mask, Dichroic and Filter wheels allow a choice of spectral and coronagraphic options in each science channel.
- An Integrated, Coronagraph Optimized Adaptive Optics (IAO) system. The role of this system is to concentrate the energy from sources in the smallest possible area so that it is more visible and picks up less background.
- Low scatter, Ghost-Free Optics. The all-reflective optical train is designed to minimize the number of surfaces and eliminate ghosts.

A functional block diagram of the NICI instrument is provided in Figure 5.

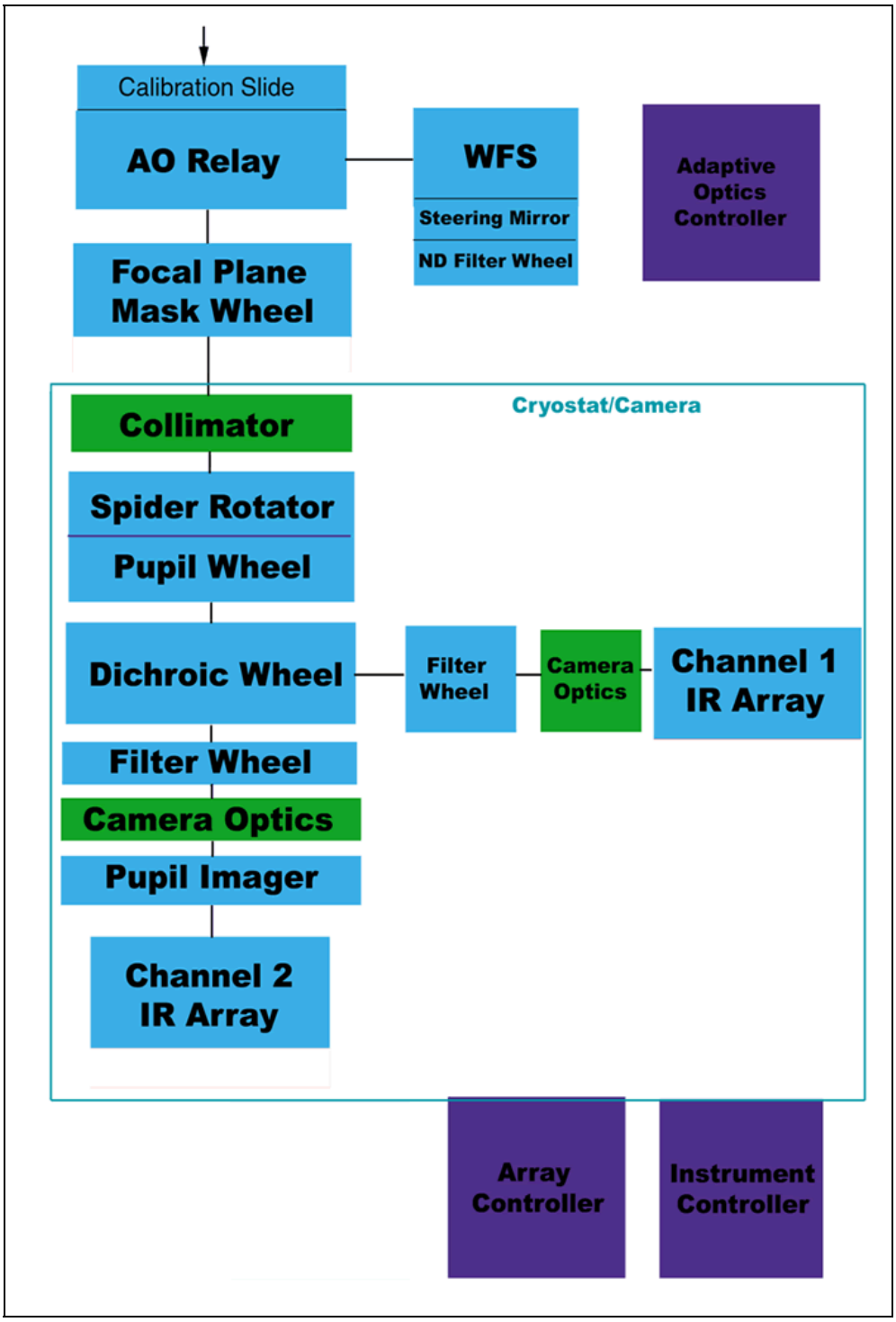

Figure 5 Functional Block Diagram of the NICI Instrument

3.1 Instrument Description

NICI consists of an Adaptive Optics Relay followed by a dual channel infrared camera. Both the AO Relay and IR camera were designed with a variety of optical elements to permit a great deal of observational flexibility. This section provides a description of the IAO system and the IR Camera. The configurable optical elements are described in the section on mechanisms, Section 3.1.3.

NICI is mounted at the Cassegrain focus of the telescope, preferably in the bottom or up-looking position, since this minimizes the number of surfaces between the instrument and the sky. For this discussion please refer to the schematic of NICI's optical layout in Figure 6.

Functionally, the instrument takes light from the telescope focus and relays it onto the deformable mirror (DM) where atmospheric phase errors are corrected. Light is then relayed onto the first instrument focal plane where one of several coronagraphic masks can be selected. There is a dichroic in the AO Relay that strips off the visible wavelength light and sends it through the AO Bench to the Wavefront Sensor (WFS). This AO dichroic has ~90% reflectivity for IR light from 1.1 - 5.4 μm and is 70% transmissive for visible light from 0.4 - 0.8 μm. The reflected science beam enters the dewar and is collimated. An image of the pupil is formed downstream of the collimator. At the re-imaged pupil, the collimated beam is masked by a choice of pupil masks, applying a variety of coronagraphic strategies.

The masked, collimated beam is then split into two beams by a number of different strategies at the cameras' dichroic wheel. This beam division can involve dichroics, filters, or neutral splits. Each of these beams is sent to an essentially identical camera. Each channel has its own selectable filter wheel to further define the beam properties. Each of the two beams is then re-imaged onto a detector. In one channel, an extra, selectable optic allows imaging of the pupil for diagnostic purposes.

The goal of the two-channel camera is to obtain images that have undergone the same atmospheric turbulence history. By finding a two channel split in which the source to background ratio varies significantly, we can isolate the source light by differencing, since one channel is always estimating the background. Between the focal plane and pupil plane mask choices, the beam division choices, and the separate filter wheels in each channel, there are literally thousands of instrument configurations possible.

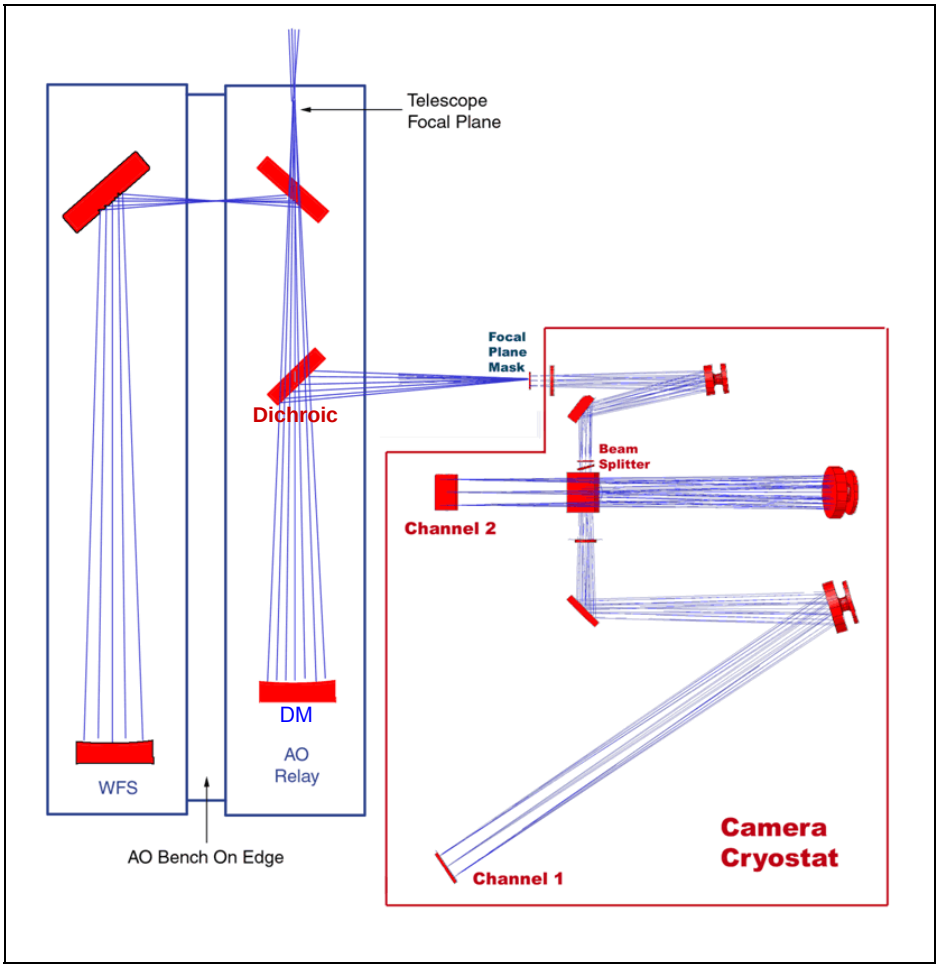

Figure 6 Optical Schematic of the NICI Instrument

3.1.1 Adaptive Optics Description

NICI's AO Relay optical layout is illustrated in Figure 7 and WFS optical layout is illustrated in Figure 8. The first instrument subsystem, the Adaptive Optics (AO) relay, images the telescope focal plane (TFP) on to the first instrument focal plane (IFP1). It consists of a pair of off-axis parabolic mirrors (OAPs), an 85 element deformable mirror (DM), a visible transmitting/IR reflecting dichroic and one flat fold mirror. The first OAP images the telescope entrance pupil onto the first instrument pupil plane (IPP1) where the DM is located. The DM reduces atmospheric phase errors based on phase information generated in the AO wave front sensor (WFS). Following the DM, a second OAP relays a corrected, real image of the telescope focal plane to the first instrument focal plane (IFP1) located just above the window of the cryostat. The visible wavelength light is separated by the dichroic and sent to the WFS off a fold mirror. The infrared light is reflected out of the plane of the paper to the cryostat.

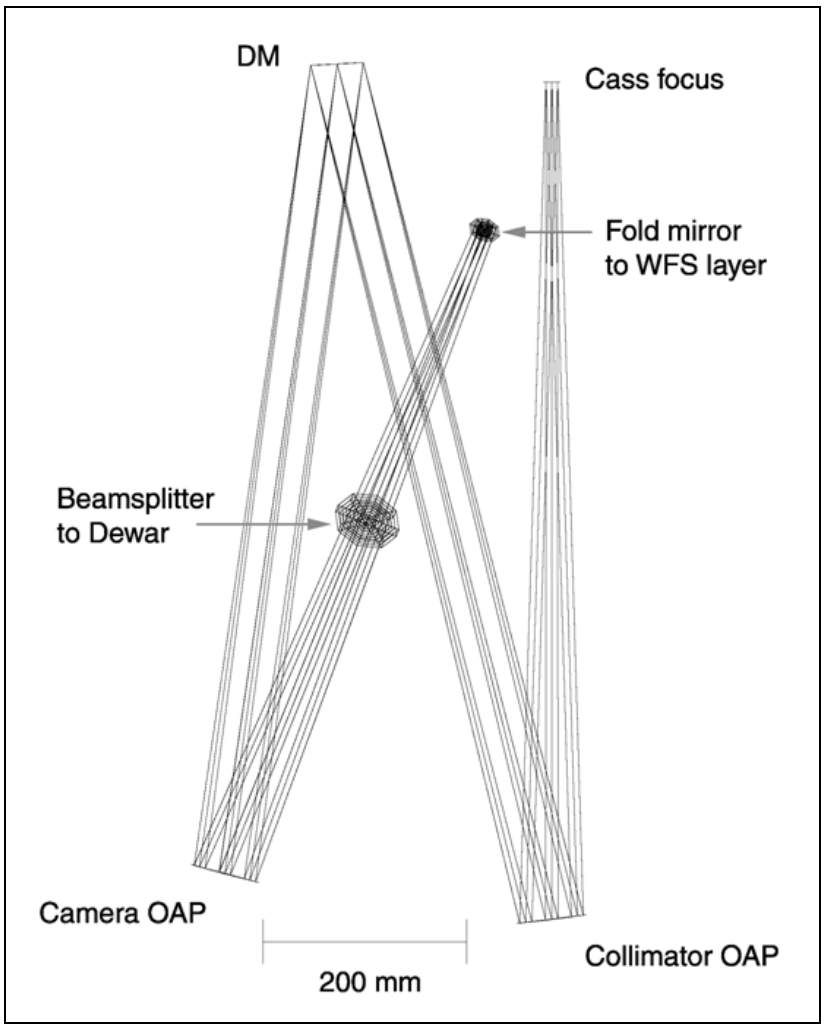

Figure 7 NICI Adaptive Optics Relay Optical Layout

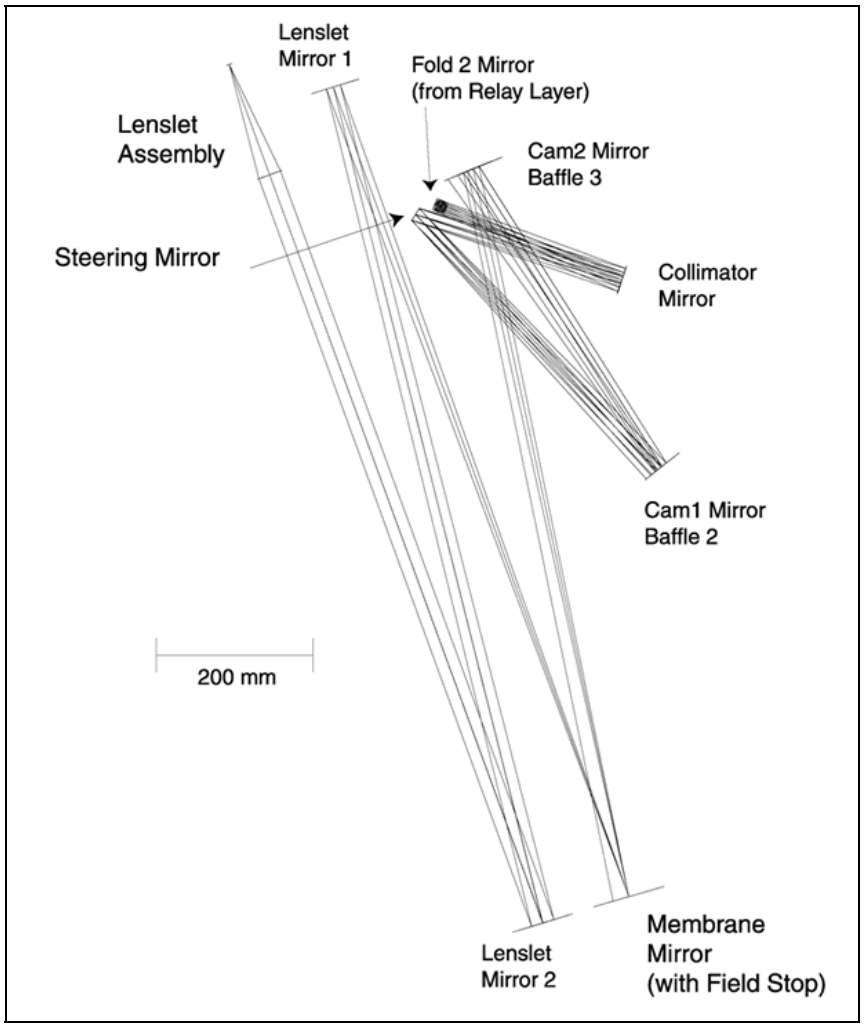

Figure 8 NICI Adaptive Optics Wavefront Sensor Optical Layout

3.1.2 Infrared Cameras Description

The Infrared beam, or science beam, is reflected off of the dichroic in the AO Relay, normal to the AO bench towards the IR Camera. The IR Camera is a re-imager with about a factor of 2.5 magnification with a dichroic split, two filter wheels and two detectors that will give simultaneous images at two wavelengths. The focal plane re-imaged by the AO Relay falls a couple of centimeters in front of the Camera/cryostat window. At this focal plane position is located a wheel with 8 coronagraphic masks. These are apodized masks on a calcium fluoride substrate. The Camera optics consist of a simple all-reflective two off-axis parabola design with two fold mirrors to isolate the pupil re-imaged by the first parabola. With the exception of the pupil imaging lens all of the mechanisms are located at or near the pupil plane between the two fold mirrors. The first mechanism is a spider mask that will reduce the spider flares in the final image plane. This mask must be rotated as the instrument rotator de-rotates the image. This is followed by the pupil plane mask wheel with a selection of 8 undersized pupil plane masks. The next mechanism is the dichroic wheel that provides a selection of 15 beam splitting options. Following the dichroic are two identical channels each with a 22 element filter wheel and a parabola to image onto the 1024x1024 1-5 micron Aladdin style array with a plate scale of 0.018 arcseconds/pixel. This gives NICI an 18.43 arcsecond field of view.

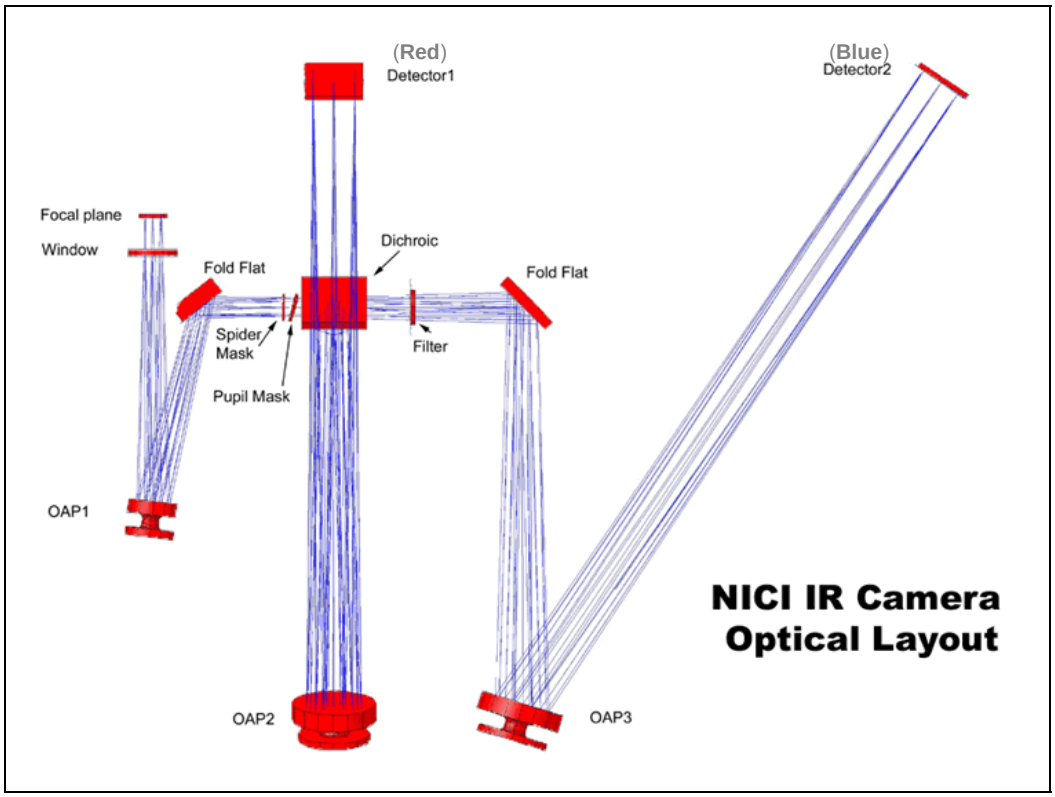

Figure 9 IR Camera Optical Layout

Read Noise (single read)	40 electrons
Read Noise (Fowler sampling)	25 electrons
Frame rate	8 Hz
Average Dark Current	≤ 1 electron/second
Well Size	200,000 electrons

Figure 10 Table of NICI Detector Properties

3.1.3 Mechanisms Description

NICI has 10 mechanisms that will be controlled by the Observer to configure the instrument for a given observation. The mechanisms permit configuration of filters, masks, pupil imaging, and dichroic elements. The table below lists the mechanisms. A brief description of each follows. For mechanisms that have spare positions, the physical specifications concerning the filters are listed in Appendix A.

Mechanism	# of Positions	Type of drive
AO Relay		
Fiber optic calibration sources	4	Four position translator
Wavefront Sensor		
Tip/tilt steering mirror	continuous	Two angle tilt mirror
Neutral density filter wheel	6	Discrete position wheel
Cryostat		
Focal Plane Mask wheel	8	Continuous rotary wheel
Spider Mask Rotator	continuous	Continuous rotary drive
Pupil Mask Wheel	8	Discrete position wheel
Beam splitter/dichroic wheel	15	Discrete position wheel
Channel 1 (Red) filter wheel	22	Discrete position wheel
Channel 2 (Blue) filter wheel	22	Discrete position wheel
Pupil imaging optics	3	Discrete position wheel

Figure 11 Table of NICI Mechanisms and Configurable Optics

3.1.3.1 Fiber Optic Calibration Source

The Fiber Optic Calibration Source (FOCS) is a four position translator mounted at the beam entrance focus of the AO Relay. It provides an internal reference source for AO calibration, distortion calibration, mapping the detectors to each other, tracking registration of the two arrays, system tests, and acts as a dust cover for the AO Relay. The fibers in all four positions are of the single mode type. The lamp that illuminates the fiber supports variable illumination from 0 to 10 V with a resolution of 8 bits and is controlled through the instrument sequencer.

- **Position 1**: This position is **one single mode fiber** mounted at the Gemini Cassegrain focus position and will be used for systems tests and adaptive optics calibration. This position also functions as a dust cover by closing the optical path. Position 1 is the **home position**.
- **Position 2**: This position has a 40 by 40 grid of 130 micron pinholes to calibrate the distortion of each channel and the mapping of one array to the other for accurate differencing.
- **Position 3**: The third position has **two IR fibers located in opposite corners** of the field of view. These two fibers can be used while taking a science image and will produce two adjustable brightness images in the corners of the arrays and will be used to track registration of the two arrays during a science observation.
- **Position 4**: The fourth position is the **open** position.

3.1.3.2 Tip/Tilt Steering Mirror

A steering mirror is required to adjust the bore sight of the AO system with respect to the IR Camera. An example would be to position the guide star at the edge of the frame. This mechanism is a tip/tilt, or two axis, mirror that is used to center the star image in the wavefront sensor's 5 arcsecond field of view. This mirror will be adjusted when dithering more than 2 arcseconds or when guiding on an off axis object. It will allow guiding over the entire 18 arcsecond diameter field. It will also be used to correct atmospheric refraction. The Tip/Tilt Steering Mirror is controlled by the user through the instrument sequencer.

The table below lists the functional characteristics of the Tip/Tilt Steering Mirror.

Maximum tilt on the sky	+/- 9 arcseconds
Step size on the sky	+/- 0.0018 arcseconds
Stability on the sky	+/- 0.0018 arcseconds
Hysteresis on the sky	+/- 0.0018 arcseconds
Maximum tilt angle at mirror	+/- 0.3 degrees
Step size at the mirror	+/- 0.2 arcseconds
Update rate	~ 1 Hz

Figure 12 Table of Tip/Tilt Steering Mirror Mechanical Characteristics

3.1.3.3 AO Neutral Density Filter Wheel

The brightness of the guide objects will range from extremely bright to very faint. This WFS wheel has 6 positions. This wheel is equipped with neutral density filters to reduce the guide star flux to levels appropriate for the avalanche photodiodes in the wavefront sensor. A red filter is included to improve signal to noise on reddish guide objects when the moon is up. The home position is a blank-off. Gemini may add another filter to the spare position. The physical specifications for the filter are provided in Appendix A.

- **Position 1**: Opaque. This is the home position.
- **Position 2**: ND4
- **Position 3**: ND3
- **Position 4**: ND2
- **Position 5**: Red filter
- **Position 6**: Spare (blank-off until used)

(This may change. We are investigating using narrow bandpass filters in place of some of the ND filters since narrowing the bandwidth should improve the WFS performance)

3.1.3.4 Focal Plane Mask Wheel

The Focal Plane Mask Wheel is mounted at the entrance to the Cryostat, before the science beam is split. The observer can choose from one of eight focal plane masks. One of the focal plane mask positions provides a calibration mask. Four positions provide standard stellar masks of different sizes. The remaining positions are for observer supplied masks. This mechanism is a continuous rotary wheel. The mask is selected by positioning the wheel to the correct position for the selected mask. One dimensional dithering is then accomplished by small movements of the wheel. The physical specifications for masks that can be populated in the user positions are defined in Appendix A.

- **Position 1**: Calibration mask (pinhole grid)
- **Position 2**: Standard stellar mask 1 0.3 arcseconds
- **Position 3**: Standard stellar mask 2 0.5 arcseconds
- **Position 4**: Standard stellar mask 3 0.7 arcseconds
- **Position 5**: Standard stellar mask 4 1.0 arcseconds
- **Position 6**: User defined mask 1
- **Position 7**: User defined mask 2
- **Position 8**: User defined mask 3

Homing accuracy	20 microns
Mask position accuracy	20 microns
Step size	2 microns
Backlash	2 microns

Figure 13 Table of Focal Plane Mask Wheel Mechanical Characteristics

3.1.3.5 Spider Mask Rotator

The Spider Mask is a cross shaped mask that aligns with the spider image in the cryostat. The mask must be rotated to stay aligned with the telescope spiders when the instrument rotates to de-rotate the field. The alignment of the spider mask is automatic. Once the observer selects that the spider mask mechanism is active, it tracks the telescope rotator position and positions itself accordingly. It will repeat this process every 60 seconds to maintain alignment. The Spider Mask Rotator is before the dichroic in the optical path, so it is common to both IR camera channels. The mechanism is a continuous rotary drive.

3.1.3.6 Pupil Mask Wheel

The pupil mask wheel allows the selection of a pupil plane mask from a choice of eight masks. The pupil plane mask stops down the outer edge and inner edge of the image of the secondary. For instance, the outer edge maybe stopped down to 90% of the full telescope pupil image. A similar area is masked around the inner hole. As the focal plane mask gets smaller the pupil plane mask needs to be more restrictive. Four of these masks are sized to cover the range of focal plane mask sizes. The other positions will be used for special purpose masks such an apodized pupil mask or a grism. The Pupil Mask Wheel is positioned before the beam is split so it is common to both IR camera channels. The physical specification for the masks that may be placed in the spare positions is defined in Appendix A.

- **Position 1**: Blank, home.
- **Position 2**: 95:5
- **Position 3**: 90:10
- **Position 4**: 85:15
- **Position 5**: 80:20
- **Position 6**: Apodized mask 1
- **Position 7**: Spare
- **Position 8**: Spare

3.1.3.7 Cryostat Beam Splitter/Dichroic Wheel

The Cryostat Beam Splitter / Dichroic Wheel has a variety of beam splitting/filtering elements that will determine which wavelengths (if any) are sent to each science channel. This allows flexibility in differential observations depending on the targeted science goals. The table below shows the planned population of the beam splitter/dichroic wheel. The project budget for these elements did not permit full population of this wheel. Additional elements may be added by Gemini at a later date. The physical characteristics of the beam splitters and dichroics that may be added to this wheel are specified in Appendix A.

Beam Splitting Elements			
Position #	**Channel 1 (Red) Response**	**Channel 2 (Blue) Response**	**Name**
1	50% over H window	50% over H window	H 50/50
2	50% over K window	50% over K window	K 50/50
Channel Splitting Elements - Dichroics			
3	≤ H	≥ K	H/K Split
Spare Positions			
4	0%	0%	Spare/Blank
5	0%	0%	Spare/Blank
6	0%	0%	Spare/Blank
7	0%	0%	Spare/Blank
8	0%	0%	Spare/Blank
9	0%	0%	Spare/Blank
10	0%	0%	Spare/Blank
11	0%	0%	Spare/Blank
12	0%	0%	Spare/Blank
13	0%	0%	Spare/Blank
14	0%	0%	Spare/Blank
15	0%	100%	Spare/Open

Figure 14 Table of Beam Splitting/Dichroic Science Channel Optical Elements

3.1.3.8 Channel 1 and Channel 2 Filter Wheels

Each science channel is implemented with a filter wheel that has 22 filter locations. Each wheel has a blank position so there are 21 available filter locations. Since the 50/50 beam splitters allow the reversing of the long and short channels, the initial complement of filters will be nearly the same in each wheel. The table below lists the layout for each science channel's filter wheel. Filters at the Spare/Blank locations may be added by Gemini at a later time. The positions not populated in the initial complement are shipped with opaque blanks. The physical specifications of filters for these wheels are provided Appendix A. These specifications will be needed should Gemini choose to add filters to the spare positions of the Channel 1 or Channel 2 Filter Wheels.

Filter Position #	Channel 1 (Red) Filter Wheel	Channel 2 (Blue) Filter Wheel
1	Blank-off	Blank-off
2	J	Spare/Blank
3	H	K
4	Spare/Blank	K'
5	Spare/Blank	L'
6	Spare/Blank	M'
7	H methane S' 1%	H methane S' 1%
8	H methane S 1%	H methane L 1%
9	H methane L 1%	H methane S 1%
10	H methane S 3%	H methane L 3%
11	H methane S 6.5%	H methane L 6.5%
12	K methane S 1%	K methane L 1%
13	K methane S 3%	K methane L 3%
14	H2O on	H2O off
15	Spare/Blank	Spare/Blank
16	[FeII]	Spare/Blank
17	Spare/Blank	Spare/Blank
18	H2 1-0 s(1)	K continuum
19	Spare/Blank	Spare/Blank
20	Br gamma	Spare/Blank
21	Spare/Blank	Spare/Blank
22	Spare/Blank	Spare/Blank

Figure 15 Table of Channel 1 and Channel 2 Filters

Filter	Response
H methane S 1%	1.5786 - 1.5945 µm
H methane S' 1%	1.5945 - 1.6110 µm
H methane L 1%	1.6180 - 1.6345 µm
H methane S 3%	1.5558 - 1.6047 µm
H methane L 3%	1.6279 - 1.6769 µm
H - H20 S 1% (feature) (H2O on)	1.4490 - 1.4630 µm
H - H20 L 1% (continuum) (H2O off)	1.5620 - 1.5780 µm
K methane S 1%	2.0850 - 2.1070 µm
K methane L 1%	2.2000 - 2.2230 µm
K methane S 3%	2.0640 - 2.1268 µm
K methane L 3%	2.2000 - 2.2670 µm
K methane S 6.5% (Gemini supplied)	1.5375 - 1.6550 µm (est.)
K methane L 6.5% (Gemini supplied)	1.6523 - 1.7495 µm (est.)

Figure 16 Table of Bandpass Filter Properties

For some differential observations observers may like to use a line filter in one channel with a continuum filter in the other channel. The following table lists suggested continuum filters for use with particular line filters.

Line Filter	Continuum Filter
FEII (1.644 µm)	H methane long 1% (1.629 µm)
H2 1-0 s(1) (2.1239 µm)	K continuum
Br Gamma (2.1686 µm)	K continuum

Figure 17 Table of Continuum Filters for use with Line Filters

Home Accuracy	+/- 0.25 mm
Detent positional accuracy/repeatability	+/- 0.25 mm
Time to rotate half the wheel	30 seconds

Figure 18 Table of Channel 1 and Channel 2 Filter Wheel Mechanical Characteristics

3.1.3.9 Pupil Imager

Pupil imaging, forming an image of the telescope entrance pupil on the array, is a function implemented in NICI. A pupil imager provides an excellent diagnostic of coronagraph performance and a very effective tool to align the Lyot stop and spider mask. The pupil imaging mode will be used initially to understand the alignment and flexure of NICI on Gemini, and will provide crucial data on the state of the telescope by showing the distribution of light at the pupil mask. The pupil imaging optics are independent and the science optics do not move when going into pupil imaging mode.

The pupil imaging mode has been included as a diagnostic function. Using the pupil imager will allow the alignment of NICI with the telescope to be checked as well as the alignment of the pupil plane mask, spider mask filters, and dichroic wheel. Normally observers will not use the pupil imager for typical science projects. This wheel has three positions, open, blank-off and pupil image. The pupil image is about 200 pixels across.

The positional accuracy of the Pupil Imager is 0.27 mm (10 pixels).

3.1.4 Electronics Description

The control electronics in NICI are comprised of two largely independent systems. One handles mechanism and array control, called Instrument Control (IC). The other controls the AO system, called AO Control. Each of these systems is housed in a separate cooled thermal enclosure, or rack. A block diagram of these racks and other major NICI assemblies is provided in Figure 19.

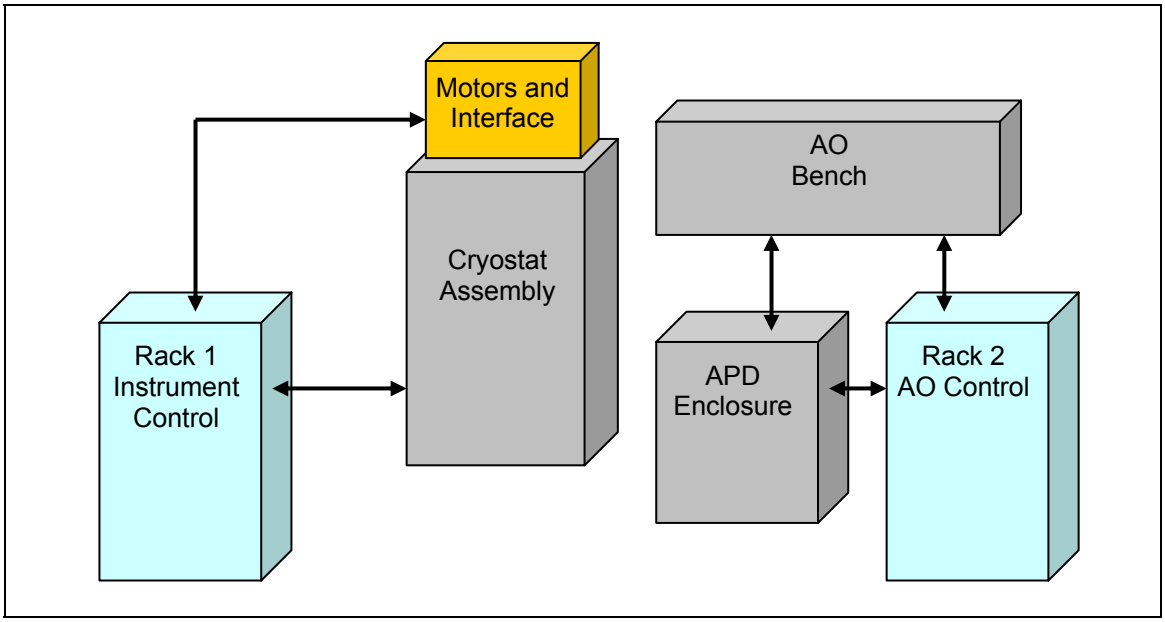

Figure 19 Block Diagram of NICI Control Racks and Major Assemblies

3.1.4.1 Instrument Control Rack

NICI's Instrument Control electronics are housed in a standard Gemini Thermal Electronics Enclosure. These electronics are responsible for array control, mechanism control, thermal conditioning of the cryostat, and image acquisition. A block diagram of the IC electronics is provided in Figure 20.

The Instrument Control Server is the primary controller for the entire instrument. It receives commands from the Gemini instrument sequencer and orchestrates the actions of the IC and AO electronics. The IC server drives the Array Controller, Pixel Servers, provides instructions for data handling to the instrument, and provides serial control over the mechanisms and temperature control subsystem.

The Array Controller is responsible for array control, clocking, and readout. The Array Controller is powered with a dedicated Array Power Supply which also powers the arrays through the Array Controller. Array clocking control is provided by digital clock signals converted to analog levels in the Array Controller and fed to the arrays in the Cryostat. The resulting analog array readout data are amplified and converted to digital pixel data by the Array Controller. The digital pixel data is fed from the Array Controller to the Red (CH1) and Blue (CH2) Pixel Servers over high speed fiber optic links. The Pixel Servers are server class multi-processor PC based computers. The Pixel Servers assemble the pixel data into frames and prepare the frames for passing to Gemini's DHS or to local disk storage.

Mechanism control is driven from the IC Server over the internal IC Rack LAN to a terminal server. Serial lines from the terminal server are fed to a Mechanism Utility Box. The Mechanism Utility Box bundles power and the serial control lines into one cable for the IC mechanisms and two separate mechanism control lines to the two AO Fiber Calibration Source translator and ND Filter Wheel mechanisms. A Junction Box mounted on the Vacuum Jacket breaks out the 7 IC Mechanism power/control lines for the individual mechanisms.

The IC Server also provides serial control over the Temperature Control subsystem via the internal LAN and terminal server. Two temperature controllers, one for each array, are used to maintain detector temperatures.

A temperature monitor provides information about the health of the cooling system in the cryostat to the IC Server.

All of the electronics in the IC Rack are powered through a remote power control module, the Ethernet Power Control. The Ethernet Power Control is accessed through telnet.

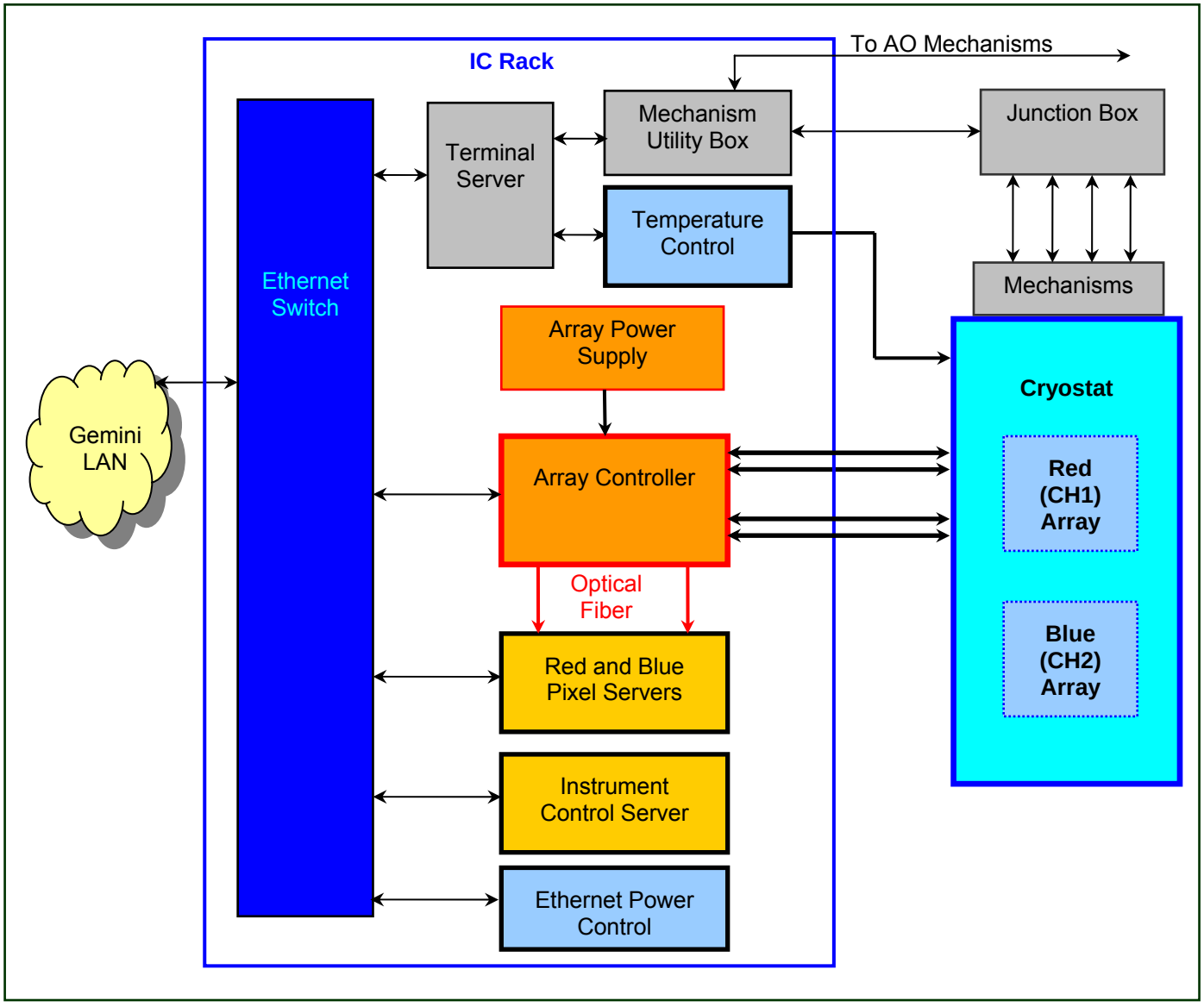

Figure 20 Block Diagram of Instrument Control Rack Electronics

3.1.4.2 AO Control Rack

NICI's AO Control electronics are housed in a standard Gemini Thermal Electronics Enclosure. These electronics are responsible for driving the AO portion of NICI. See Figure 21 for a block diagram of the AO Control electronics.

The major electronics parts of the AO Control electronics are a Real-Time (RT) Server, a User Interface (UI) Server, High Voltage Amplifier (HVA) Chassis and Counter Chassis, a steering mirror PZT controller, Remote Power Control (RPC) modules, and a terminal server (DIGI Portserver). All of these subsystems reside in the electronics thermal enclosure, except for the UI Server, which is located in the facility. The optical components that are directly controlled by the electronics are the Wavefront Sensor (WFS), the Membrane Mirror (MM), Deformable Mirror (DM), a tip/tilt platform. The Field Steering Mirror (FSM) and Neutral Density Filter Wheel (NDFW) are controlled by the electronics in the IC Rack.

The AO control loop starts with the lenslet array (LLA). Two out of focus images are generated on the LLA by a Membrane Mirror (MM). Photons passed by the lenslet array are converted into TTL pulses by Avalanche Photo Diode modules in the WFS. These pulses flow through 85 coaxial cables from the APD enclosure to the Counter Chassis. Here the pulses are integrated and sent to the RT Server via a fiber optic cable. The RT Server calculates the wavefront errors and the DM and TT platform error signals. These error signals are sent to the HVA Chassis via another fiber optic cable. The HVA chassis converts the error signal into high-voltage signals to drive the DM. Software communicates with the Counter Chassis to generate corrections to the TT platform. The Digi Portserver provides an interface to the Remote Power Control modules and permits monitoring of an APD Temperature Sensor.

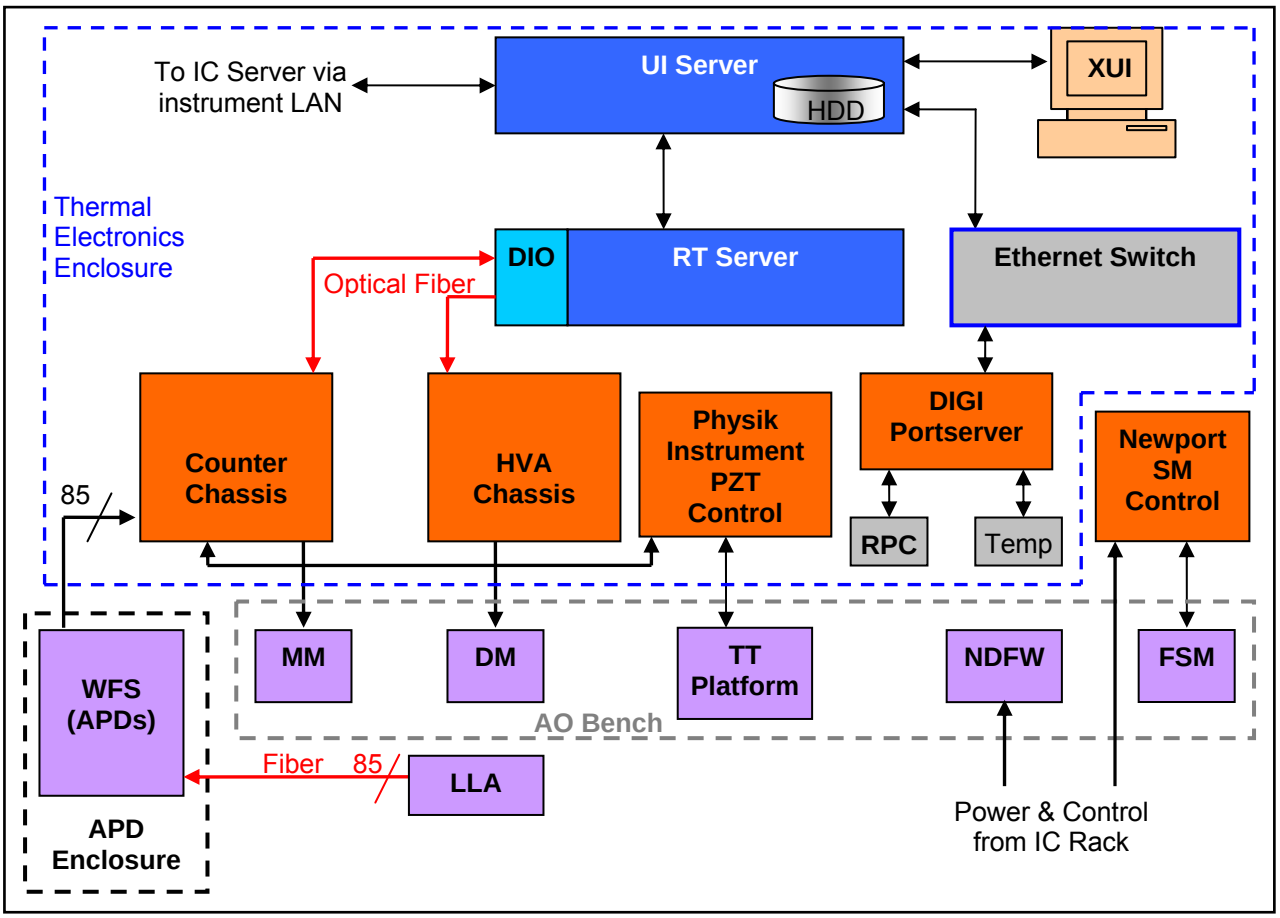

Figure 21 Block Diagram of AO Control Rack Electronics

4 Important Aspects of Operation

NICI was designed first and foremost as an instrument to do differential imaging in a coronagraphic mode fed by its own AO system with the main emphasis on methane absorbing planets near a star. As such use of NICI differs from standard imagers in a few ways that are significant. The purpose of this section is to highlight aspects of NICI that should be considered by observers when planning to use NICI for their observations. These aspects will be discussed as concepts, not giving specific commands. The specific controls of NICI will be discussed in Section 6 Gemini Operation.

4.1 Core Science Modes

While NICI will be enable many types of observations the design was strongly driven by methane differential imaging near bright stars. Other desired observational modes were not allowed to compromise this core science goal. The details of how this goal drove the instrument design are presented in the NICI OCDD and FPRD. Some of the keys points in the NICI design are listed below.

4.1.1 Narrow Fields

NICI will make significant advances in imaging within a few arcseconds of bright stars. Since the images fed to the camera will be AO enhanced, pixel sampling of .018 arcseconds per pixel were required to critically sample the ~.036 arcsecond image cores. This results in a field of view of only 9 arcsecond radius. While this is a small field it is not expected to affect the core science which will be focused on the inner few arcseconds.

4.1.2 Speckle Shear

Speckles scale radially with wavelength. Even with narrow filters placed shoulder to shoulder the speckle shifting or shear between the two wavelengths and two images is on the order of 10% of the image core. This has driven NICI to have very narrow (~1%) filters that are very close together. Since the dominant noise source around the star will be speckle driven and not shot noise, NICI had to be designed to maximize the cancellation of the speckles.

4.1.3 50/50 Beamsplitter

Because the filters are very close together in wavelength it was not possible to design a dichroic that could transition quickly enough. For this reason the prime infrared beamsplitter is not a dichroic but a 50% reflective 50% transmissive beamsplitter. This throws away half of the light which is a large negative but allows the filters to be as close as desired and they may even overlap. The 50/50 beamsplitter also allows the short and long wavelength channel to be reversed which will help discriminate real detections from systemic problems.

4.1.4 Narrow Filters

The key focus has evolved to be differential methane imaging in the H window (as opposed to the K methane feature). The reasons for this involve increased light at H, smaller images, and most importantly the methane feature is very deep with very steep transitions which allow the filters to be closer together. One difficulty in specifying the filters was that some of the objects that we wish to detect, like very cool T dwarfs, have no observed spectra to use as a model as of yet. We based the filter specifications on observations of warmer objects, Jupiter and models of cooler objects. The methane feature in the H window is conveniently about 1.5% wide which is a good match to the narrowest good transmission filters of 1%. The methane absorption registers well with all objects and models. The center wavelength of the optimum continuum filter varies by object so two have been supplied in NICI. One is matched to the peak shortward of the methane feature of the T5 observations and the other slides closer to the absorption based on the model. As objects are discovered and their spectra observed, these filters may well need to be redesigned. The following three figures show the issues discussed in this section.

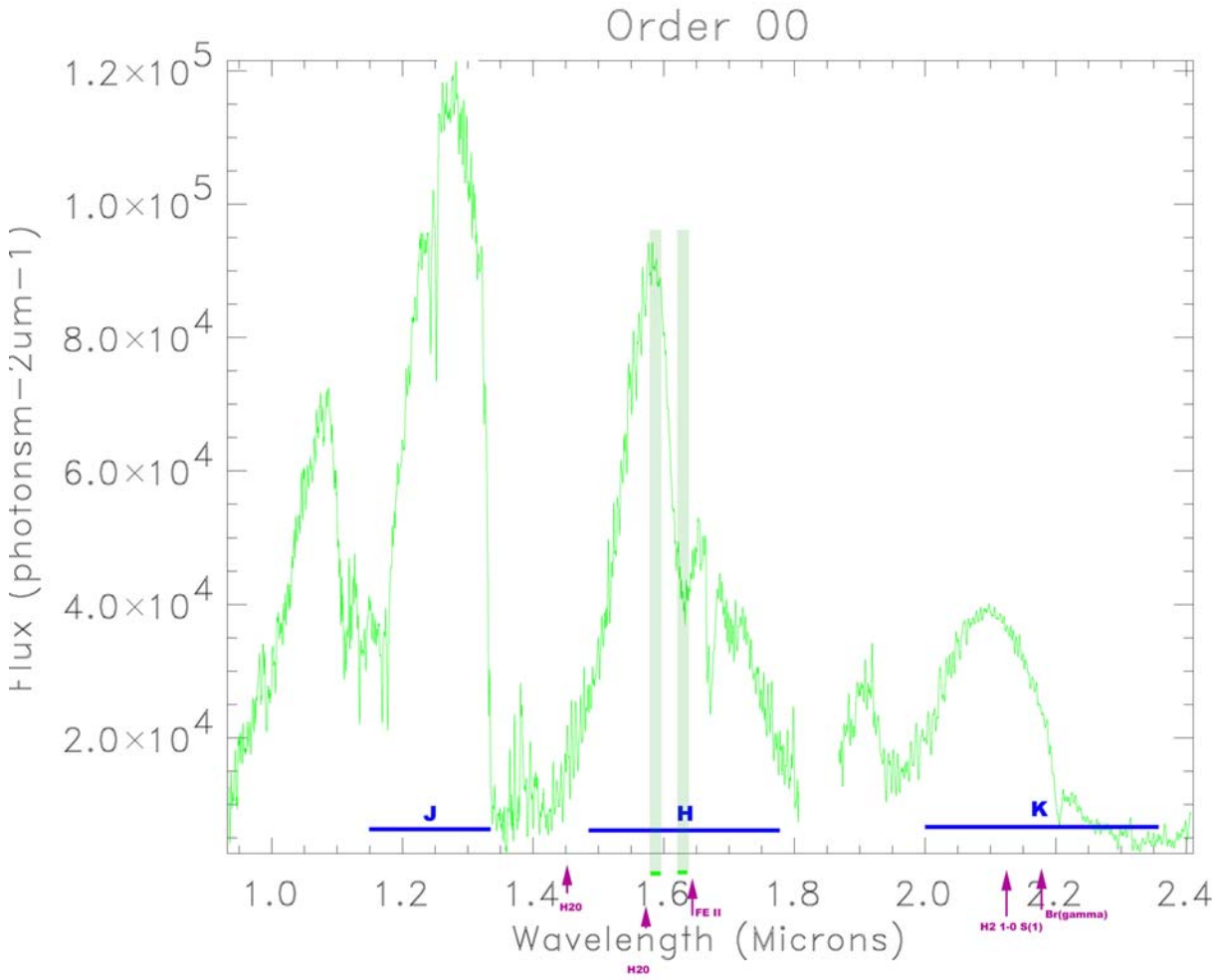

Figure 22 T5 spectra taken with SPEX on the IRTF showing optimal 1% filter

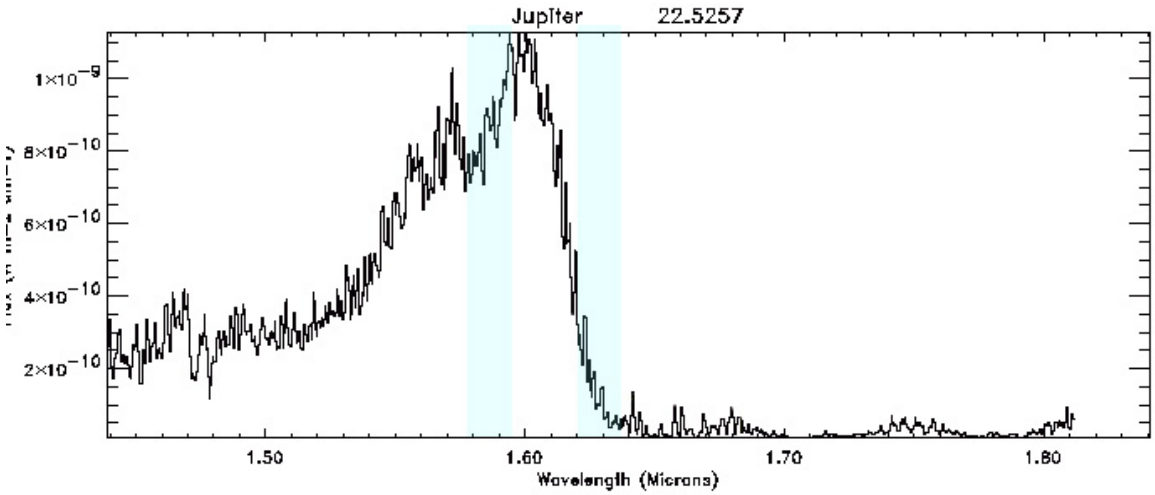

Figure 23 Jupiter spectrum taken with SPEX on the IRTF showing how the T5 filter would align on Jupiter

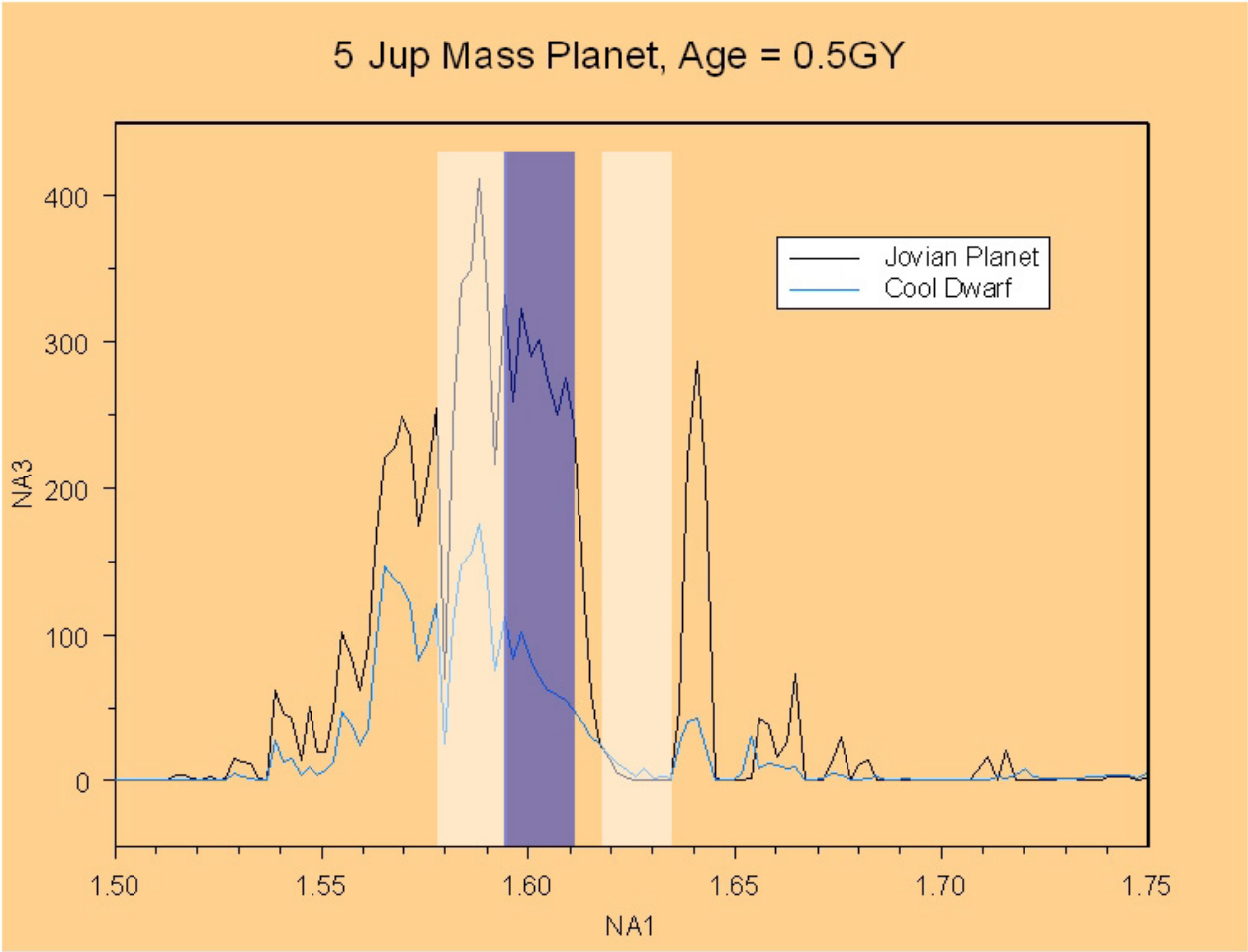

Figure 24 Filters shown on the Burrows model of a Jovian Planet and a Cool Dwarf – White band is the T5 optimized filter and the blue band is a filter optimized to be closer to the absorption feature

4.1.5 Simultaneous Array Readout

Since differential imaging is central to the NICI scientific approach and since speckle noise will be the dominant noise source close to the star it is crucial that the two images to be differenced record the same time period accurate to about 1 ms. Therefore the NICI array controllers have been design to readout simultaneously to greater than 1 ms accuracy. Channel one is the master and channel two is the slave. When in simultaneous mode a Go command sent to channel 2 will enable that channel but not start the integration. A Go sent to channel one will then trigger both channels to integrate and readout simultaneously. This means that for optimum performance in this mode integration times, the number of coadds, and the number of NDR reads must be the same for both channels. This will result in slightly different flux levels in the two channels that will have to be scaled in the reduction before differencing.

4.1.6 Coronagraphic Masks

The coronagraphic masks in NICI are selected in pairs. That is, a focal plane mask of a certain size will be best matched to a specific pupil mask. The larger the focal plane mask the less restrictive the pupil mask needs to be. If imaging very close to the primary is desired a more restrictive pupil mask will be needed which will result in a lower throughput. The point here is that the observer will have to choose which masks best suit their program and understand the trade-offs involved. The performance with the different masks will be measured during the commissioning and results will be available to observers to guide their selection.

4.1.7 Dithering

Since good flat fielding is very important to the data quality from NICI a provision has been made for small dithers in one dimension. Dithering with NICI is a complex matter however. Once the AO loop is turned on the AO system will keep the star on the mask even if the telescope is moved so offsetting the telescope will not affect a dither. To dither the steering mirror in the AO wavefront sensor must be tilted to offset the AO guide point. The focal plane mask must be moved in a coordinated move to put the mask at the new star position. Dithers are expected to be only on the order of 1 arcsecond since the radius of the field is only 9 arcseconds. The focal plane mask is mounted in a wheel and is moved by rotating the wheel, thus dithers can only be done in one dimension and will follow a slight arc. This will all be handled in the software but the observer should be aware that dithers will be only possible along this arc.

4.2 Array Operation

Since NICI has very small pixels the integration times will not be very short. At shorter wavelengths integration times will be on the order of 1 to 2 minutes. In the thermal wavelengths the integration times will be more on the order of 1 to 2 Hz. Since very fast integrations are not required there are not very many options that must be adjusted in the array controller. The issues that an observer needs to be concerned with are listed below.

4.2.1 Simultaneous Start

NICI is equipped with hardware triggered science array controllers so that images from both arrays will be simultaneous to less than 1 millisecond. A Go command to channel two enables that channel but integration does not start until a channel 1 go is executed then both channels start integrating simultaneously.

4.2.2 Well Depth

For most operations with NICI a low well depth will be used to optimize the array performance. At longer wavelengths such as L and M or for very bright stars deeper wells will be required. The well depths provided are low, medium, and high. Selecting a well depth changes the reset level on the array. Large wells create more hot and bad pixels. The voltages that correspond to each well can be modified through the array controller engineering interface.

4.2.3 Slow/Fast Clocking Pattern

The array controller is capable of fast and slow clocking patterns. The fast pattern is optimized for speed and has increased noise. The Slow pattern is optimized for low noise. The slow pattern is planned to be used in all NICI modes but the fast pattern is selectable through the Array controller engineering interface.

4.2.4 Double Correlated Reads

The array controller is capable of signal minus pedestal (arc_D, correlated double sampling) and signal only reads(arc_S, single reads) this is selectable through the Instrument Sequencer but it is envisioned that signal minus pedestal reads would always be used.

4.2.5 Noise Reduction Reads

The array controller is capable of multiple reads to reduce the read noise called NDR reads. The number of NDR reads can be set through the IS.

4.2.6 Subarray Operation

Subarrays can be used to get shorter integration times for very bright stars if the entire filed is not required. This is settable through the IS.

5 Observing with NICI

The scientific projects that will be addressed with NICI will vary greatly in scope. The core science projects, however, can be represented by a small group of Observing Scenarios that will be described in detail later in this section. These observing scenarios will be used to explore in detail how NICI can work and how an observer can use NICI. This section details operations and issues directly relevant to observers.

5.1 Envisioned Operation

In most ways NICI will operate as most Gemini instruments. However, due to its nature NICI will be a bit more hands on in operation than most of the other instruments. Two of the key reasons for this are AO operation and the complexities of operating a coronagraph. These interactions are not difficult and can be handled by the SSA or a Support Scientist. These two aspects are discussed in the following two sections.

5.2 Adaptive Optics Operation

The operation of the AO system is described in detail in the AO users manual. This section is meant to familiarize a user with the operation issues.

The operation of the AO system is similar to that of a guider. Suitable counts are needed in order for the WFS to properly measure the wavefront errors. This will mean adjusting the ND filters or narrow band filters for the chosen guide star which in most cases will be the target object primary star. Two additional parameters that will need to be adjusted are the loop gain and the optical gain. Loop gain is the fraction of the measured wavefront error that is added to the loop integrator for each loop of the AO servo. This is typically 0.2 to 0.7 depending on the guide star brightness and the seeing conditions. The optical gain is controlled by the membrane mirror throw which affects the measured curvature of the WFS. Adjusting the membrane mirror throw changes the extra focal distance of the out of focus images that the WFS uses to measure the wavefront curvature. The closer this is to the focus (greater membrane mirror throws) the higher the optical gain. The extra focal distance must be greater than the curvatures that are present otherwise they will not be measured. In bad seeing the membrane mirror throw must be reduced. While it is hoped that the membrane mirror stroke determination can be reduced to an automated measurement and calculation, initially it will be set manually.

The AO XUI will be used to determine if AO is properly setup and that the loop is running nominally. The AO XUI is shown in the Figure 25. The first pie shaped diagram shown in the upper left of the XUI displays the total signal counts from both phases of the AO Loop. This represents the total signal level and will give the operator the information needed to determine if the star is too bright or if there are marginal counts. If the counts are too high (too bright), a thicker ND filter will be required. If the counts are too low the AO parameters will have to be adjusted to reduce the AO bandwidth.

The second pie shaped diagram shows the curvature signal. With a little training the operator will be able to identify problems by looking at this display. An object that is decentered will cause the curvature diagram to look dark on one side and bright on the other. An out of focus star will look all bright or all dark. When the loop is running properly the curvature signal will be low in all channels.

The diagram in the top right shows a bar graph of the corrections being sent to the deformable mirror. Again with a little practice tilts and focus errors are obvious in this display. More importantly an experienced eye can tell if the loop is operating happily or if something is wrong by looking at the mirror correction fluctuations. The fourth diagram shows a triangle that indicates the state of the tip-tilt stage behind the deformable mirror.

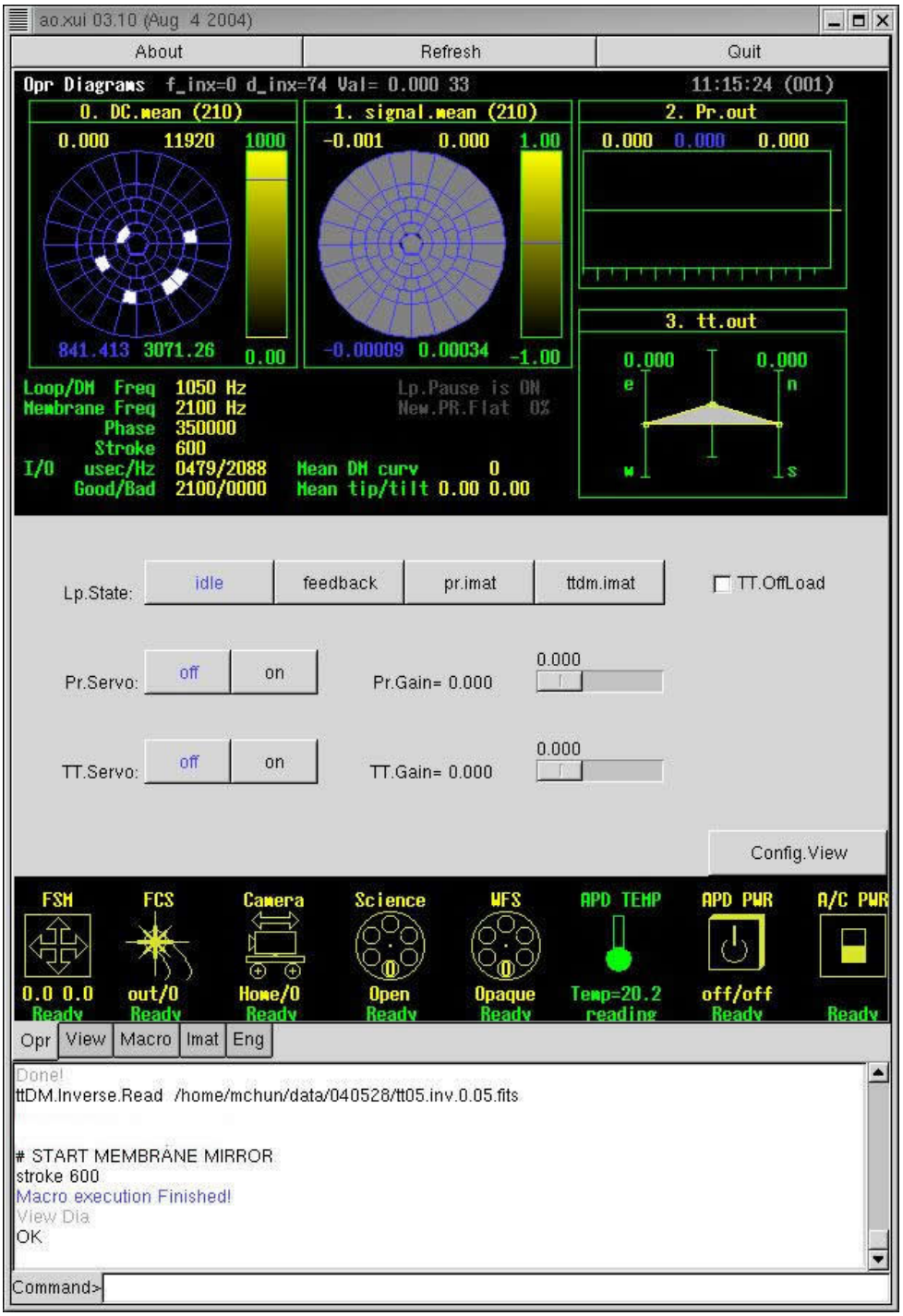

Figure 25 Screenshot of the AO XUI

5.3 Coronagraph Operation

The photon rate at the science array depends much more on the seeing conditions with a coronagraph than with a simple imager. The amount of light that gets around the focal plane mask will change substantially as the PSF expands. At times it will be necessary to adjust the integration times and even focal plane mask sizes to adjust to the seeing conditions. Faint guide stars that degrade the AO performance will cause a similar effect.

5.4 Preparation for Observing

This section describes the planning and procedures for preparation for observing. The steps are listed as conceptual commands. Specific commands and how they are executed are discussed in section 6.

5.4.1 Pre-Run Planning

This section provides an overview of what observers may like to do before a night of observation.

1. Select a list of science objects.
2. Find stars for the PWFS using the Gemini Observing Tool.
3. Determine a sky position that can use the PWFS probe science position.
4. Determine if the central star is sufficient for IAO use.
5. Determine ND filter need for the OIWFS from a table given the brightness and spectral type of the guide star.
6. Deselect objects that have poor guide options from list.
7. Select Focal Plane Mask, Pupil Mask, Dichroic, Channel 1 (Red) Filter, and Channel 2 (Blue) Filter for each observation.

5.4.2 Daytime Camera Setup, Calibration and Checkout

This section provides an overview of daytime tasks for setting up the science cameras, calibration, and checkout. The procedure outlined here includes mapping calibration of the arrays and determining focal plane mask location. Different masks and particularly user masks may not be located at the same pixel on the science arrays and therefore must be measured.

1. Set the Pupil Mask to 90:10.
2. Set the Focal Plane Mask to Open.
3. Set the Dichroic to 50/50 H.
4. Set the Channel 1 (Red) Filter to h.
5. Set the Channel 2 (Blue) Filter to h.
6. Set the Fiber Calibration Source to the Pin Hole Grid.
7. Turn on the Gemini calibration unit to provide an extended illumination for the H filter
8. Set integration parameters on both channels to 1 second.
9. Set the FITS comment field to "Mapping Calibration".
10. Take and save the mapping calibration image with both arrays.
11. Determine the offset and rotation for quick look parameters.
12. Set the Focal Plane Mask to 0.3 arcseconds.
13. Set the FITS comment field to "Mask Location".
14. Take and save the mask location images with both arrays. (GCU still on)
15. Determine the position of the center of the mask.

5.4.3 Daytime AO Setup, Calibration and Checkout

This section provides an overview of daytime tasks for calibration and checkout of the AO system. The procedure outlined here is aimed at determining the bore sight and setting the AO steering mirror to center the AO sweet spot on the middle of the focal plane mask.

1. Set the ND Filter Wheel position to ND4.
2. Set the Fiber Calibration Source to Single Fiber.
3. Set the Steering Mirror to the home position.
4. Set AO focus offloading to off.
5. Set AO tilt offloading to off.
6. Check the APD counts. The photon count rate should be below 1000 counts per APD per 2 KHz AO cycle (MM frequency). Exceeding this limit may critically damage the APDs.
7. Set the AO loop to on.
8. Set the Pupil Mask to Open.
9. Set the Set the Focal Plane Mask to Open.
10. Set the Dichroic to H 50/50.
11. Set the Channel 1 (Red) Filter to H Methane S 1%.
12. Set the Channel 2 (Blue) Filter to H Methane L 1%.

13. Set the integration parameters to 10 seconds
14. Set the FITS comment field to "Bore sight".
15. Take and save bore sight images with both arrays.
16. Determine the position of the FCS image and compare to the center of the mask determined in the procedure defined in Section 5.4.2.
17. Adjust the steering mirror to put the FCS source image on the pixel identified as the center of the mask.
18. Record the nominal bore sight center position for the steering mirror.

5.5 Night-Time Calibration and Setup

In between science objects, and for each setting of filters or dichroics, the facility calibration unit will be used to take flat fields. These will be used in addition to the sky flats until the optimal field flattening is determined.

5.5.1 Twilight Setup

This section describes tasks to be performed just prior to night time. The procedure below sets Pupil Mask and Spider Mask allignment, centers the guide star on the OIWFS, and sets the Spider Mask zero point.

1. Slew the telescope to a sky position near the science object.
2. Position the PWFS probe for the selected guide star.
3. Set the instrument rotator at a 0 degree position angle.
4. Set the instrument rotator to de-rotate the image.
5. Set the Spider Mask Rotator to active.
6. Select the Pupil Imager mode.
7. Set the Channel 2 (Blue) Filter to L'.
8. Set integration time to 0.1 second and 1 co-add.
9. Set the FITS comment field to "Spider Mask".
10. Take a setup image to check Pupil Mask and Spider Mask alignment.
11. Verify that the Spider Mask position covers spiders and adjust if necessary.
12. De-select pupil imaging mode.
13. Slew to the science object.
14. Reacquire stars for the PWFS.
15. Set the OIWFS Steering Mirror to the nominal bore sight position as determined in the Daytime AO Setup procedure in Section 5.4.3.
16. Set the OIWFS ND Filter for the selected guide star.
17. Set the Channel 2 (Blue) Filter back to the selected science filter.
18. Activate the AO system with default parameters.
19. Take an image in Channel 1 and send to the DHS for centering analysis.
20. Adjust the OIWFS Steering Mirror accordingly.
21. Record the OIWFS spatial zero points and set new bore sight position.
22. Determine and set optimal AO servo parameters.
23. Take an image with Channel 1 to view spider flares sent to Quick Look.
24. Adjust the Spider Mask zero point to minimize spider flares.
25. Set the new Spider Mask zero point.

5.5.2 Flats with Facility Calibration Unit

This section describes how to acquire flat images with the facility calibration unit.

1. Pause the AO system.
2. Set the facility calibration unit to black body mode.(TODO Need to determine parameters)
3. Set integration parameters in both channels. (TODO Need to determine integration time)
4. Set the FITS comment field to "Flat".
5. Select 10 coadds
6. Take and save flat science images in both channels.
7. Set the integration parameters to 2 times initial integration time
8. Take and save flat science images in both channels.

5.5.3 Sky Flats

1. Pause the AO system.
2. Offset the telescope to a sky position
3. Set the integration time to XXX seconds and 10 co-adds. (TODO Need to determine XXX)
4. Set the FITS comment field to "Sky Flat".
5. Take and save sky frames.
6. Verify that no stars are present in the sky field with the quick look display
7. Dither position and repeat 4 times.

5.6 Science Observations: Modes and Scenarios

The procedures for science observations will vary with the type of observing project being conducted. This section is meant to provide direction for several common observational scenarios. Of course NICI is not limited to just these observing modes and scenarios. They are meant as a guideline. Specific instructions are provided for the following observing scenarios:

- Spectral differential imaging with dithering
- Point spread function differencing
- Photometry of a faint companion with dithering

5.6.1 Spectral Differential Imaging with Dithering

Differential imaging is certainly not new to infrared astronomy. Traditional beam switching and sky subtraction is a differential imaging method. The difference with NICI will be that the differential imaging will be simultaneous, and that the difference will be between images at two wavelengths. This reduces the importance of the sky images, which will now be used as a processing aid, and at times for a flat field. Objects will typically be stared at for long periods of time (up to 2 hours) and sky frames taken about 10% of the time.

Dithering is also a bit different with NICI. Typically, observers will dither in a two dimensional pattern with steps of 2-5 arcseconds or more. NICI has such a small field of view of view that a plus and minus five arcsecond dither would throw away about half of the field. With NICI, the dithers will be small. Typical dithers will be about an arcsecond. Additionally, the dithers will be in an arc as defined by the rotation of the focal plane mask wheel. This is in a sense a 1 dimensional dither.

Examples of the projects this type of observing method would be used for are methane companion searches, brown dwarf age measurements, and imaging of ionized outflows from YSOs. The following is a typical observing sequence for Differential Imaging with Dithering where a source is found. This is the “kitchen sink” scenario and will exercise every aspect of the instrument.

5.6.1.1 Setup Prior to Observation

These steps should be executed prior to observation.

1. Set the Fiber Optics Calibration Source to position 3, corner fibers, to produce two faint spots in the corners of the science arrays to provide registration data while integrating
2. Set the Pupil Mask Wheel to blank.
3. Set the AO ND Filter Wheel to blank.
4. Set the OIWFS Steering Mirror to the nominal bore sight
5. Set the PWFS to the guide star position.
6. Slew the telescope to the science object.
7. Acquire the guide star with the PWFS.
8. Set the ND Filter for guide star brightness.
9. Set the AO Membrane Mirror stroke.
10. Set the AO loop gain.
11. Turn the AO loop on.
12. Check for excessive APD counts. The APDs must have less than 1000 counts per APD per 2 KHz cycle (MM frequency). Adjust the ND Filter Wheel if necessary. Exceeding this count could critically damage the APDs.
13. Enable AO Tip/Tilt offloading.
14. Enable AO focus offloading.
15. Set the Focal Plane Mask to 0.3 arcseconds.
16. Set the Dichroic to H 50/50.
17. Set the Channel 1 (Red) Filter to 1% H methane on.
18. Set the Channel 2 (Blue) Filter to 1% H methane off.
19. Set the Pupil Imager to open.

20. Set low array bias on both arrays.
21. Set the integration time to 60 seconds.
22. Set other array parameters (subarray, CDS, NDRs, rtime).
23. Set co-adds to 1.
24. Set the FITS comment field to indicate the science object name.
25. Select the desired sky rotation and command the OCS to de-rotate the image.
26. Enable the Spider Mask Rotator to track.
27. Set the Pupil Mask Wheel to 90:10.
28. Set the DHS destination to quick look.
29. Send the Go command to Channel 1.
30. SSA, adjust centering if the star is not centered on the focal plane by adjusting the steering mirror.
31. Repeat frame captures in Channel 1 and adjustments until centered.
32. Set atmospheric refraction correction to on (in the instrument sequencer)

5.6.1.2 Capturing Science Data

This procedure of capturing science data will be repeated 4 times in conjunction with capturing sky frames.

1. Capture science frames and save the DHS, sending to quick look. (~5 frames at 60 seconds each = ~5 minutes).
2. Take sky frames (see 5.5.1.3)
3. Dither to position #2. Move OIWFS Steering Mirror, Focal Plane Mask, and PWFS probe to desired dither amount in a simultaneous move.
4. Capture science frames as in step 1. (~5 minutes)
5. Take sky frames.
6. Dither to position #3 as in step 2.
7. Capture science frames as in step 1. (~5 minutes)
8. Take sky frames.
9. Dither to position #4 as in step 2.
10. Capture science frames as in step 1. (~5 minutes)
11. Take sky frames.
12. Dither to position #5 as in step 2.
13. Capture science frames as in step 1. (~5 minutes)
14. Take sky frames.
15. Dither to position #6 as in step 2.

5.6.1.3 Sky Frames

The procedure of capturing sky frames will be performed 4 times in conjunction with capturing science data.

1. Pause the AO loop.
2. Offset to a sky position.
3. Set the integration time the same as for the science object.
4. Set the FITS comment field to "Sky"
5. Capture sky frames. (~5 minutes).
6. Return to science object position.
7. Reacquire the guide star with the PWFS.
8. Set the AO loop to on.

5.6.1.4 Flats with Facility Calibration Unit

1. Pause the IAO loop.
2. Set the facility calibration unit to black body mode.
3. Set integration time XXX seconds for flat. (TODO determine XXX)
4. Set the FITS comment field to "Flat".
5. Set the DHS destination to quick look.
6. Capture flat science images in both channels.
7. SSA, verify levels are correct for flats on quick look.
8. SSA, adjust integration time if required.
9. Set the number of co-adds to 10.
10. Set the DHS destination to save and to quick look.
11. Take flat science images in both channels.
12. Set the integration time to twice the initial time.
13. Take flat science images in both channels.

5.6.1.5 Mapping calibration (used for mapping one array to the other before differencing)

This procedure should be done before and after the science observation. For very long periods on one object or when tracking through zenith the frequency of this calibration may need to increase.

1. Set the Fiber Calibration Source to the Pin Hole Grid.
2. Turn on the Gemini Calibration Unit to provide an extended illumination for the H filter
3. Set integration parameters on both channels to 1 second.
4. Set the FITS comment field to "Mapping Calibration".
5. Take and save the mapping calibration image with both arrays.

5.6.2 Point Spread Function Differencing

When there is no reasonable spectral feature that allows the spectral differencing mode to be used images will be taken in two filters such as H and K, or L and M, and then differenced with a nearby reference star. While a less sensitive and less powerful observing mode than the simultaneous modes, this will still be important observing mode. A typical project would be the imaging of optically thick disks around other stars. The dusty disks have no strong spectral features. That allows the cancellation of the residual stellar light, and must be differenced with a sequentially observed star to remove the residual halo, leaving only the light from the disk.

Best results are achieved with a reference star that has no known infrared excess, which is similar in brightness and color to the target star, and is very close to the target star. The telescope will be offset between the two stars on a time scale that is short enough to allow the PSF to be similar and long enough not to drastically impact the integration duty cycle. Typical switching times would be on the order of five minutes over a period of two hours, resulting in 24 pairs. Each pair may be comprised of up to five images of each object, for a total of 240 images.

Sky frames will be taken about ten percent of the time to be used in data reduction. Sky frames from the whole night or run are combined to produce a flat.

This scenario assumes that the setup prior to observation sequence in Section 5.6.1.1 is just complete. This means that the star is centered on the mask and the IAO loop is on and locked on the guide star, the spider mask position is active, and atmospheric refraction correction is on.

1. Select the 0.15 arcsecond focal plane mask
2. Select the 85:15 pupil mask
3. Select the K/L dichroic
4. Select Channel 1 (Red) filter K.
5. Select Channel 2 (Blue) filter L'
6. Set the integration time for Channel 1.
7. Set the integration time Channel 2
8. Adjust the number of co-adds to yield the same total integration times in each channel.
9. Set the FITS comment field to the science object name.
10. Capture and save science frames.
11. Pause the AO loop.
12. Offset the telescope to the reference star.
13. Set the PWFS to a position for the reference star.
14. Acquire the guide star with the PWFS.
15. Set the AO loop to on.
16. Adjust integration times if required for the reference star.
17. Set the FITS comment field to the reference object number.
18. Capture and save science frames.
19. Dither position with the steering mirror. Offset and repeat the capture.
20. Pause the AO loop.
21. Offset the telescope to the to the science object.
22. Reset the integration times for both channels if they were changed for capturing the reference star.
23. Set the PWFS to position for the science object.
24. Reacquire the guide star with the PWFS.
25. Turn the AO loop on.
26. Repeat science frames offsetting between objects.
27. Offset to the sky every 5 cycles and take a sky sequence.
28. Before and/or after the full sequence of captures, capture flat frames as above and mapping data (sections 5.5.1.4 and 5.5.1.5)

5.6.3 Photometry of a Faint Companion with Dithering

The discovery mode of NICI will be very powerful for finding new objects to study but this mode represents only the start of the real science. Merely finding a faint object or extension next to a star is not enough. Quantities must be measured about the discovery in order to make meaningful progress toward understanding these systems. Accurate spectra and photometry are crucial for this progress.

Photometry of a faint companion is similar to traditional photometry except that the dominant background is not from the sky or the telescope but from the parent or central star. As with the spectral mode the observing technique must enable the removal of the residual background from the star so as not to corrupt the photometry.

Since this observing mode is not a differential mode, sky frames will be taken in the normal fashion.

This scenario assumes that the Setup Prior to Observation sequence in Section 5.5.1.1 is just complete. This means that the Science object is centered on the mask and the IAO loop is on and locked on the guide star, the spider mask position is active, and atmospheric refraction correction is on.

Other flux standards and extinction stars will be done in the same way as the flux standard below. Flat fields would be taken by preferred method or made from stacking up the sky images.

1. Select the .3 arcsecond focal plane mask.
2. Select the 90:10 pupil mask.
3. Select the H/K dichroic.
4. Select the Channel 1 (Red) filter H.
5. Select the Channel 2 (Blue) filter K.
6. Set the instrument rotator to de-rotating image.
7. Set the integration times and number of co-adds for Channel 1 (Red) and Channel 2 (Blue).
8. Set the FITS comment header to the science object name.
9. Capture and save science frames. (60 seconds)
10. Pause the AO loop.
11. Set the FITS comment field to "Sky".
12. Offset the telescope to the sky position.
13. Capture and save sky frames. (60 seconds)
14. Offset the telescope to the science object.
15. Set the FITS comment field to the science object name.
16. Capture and save science frames.
17. Repeat the object/sky captures 5 times.
18. Dither the position.
19. Move the OIWFS Steering Mirror the desired dither amount.
20. Move the Focal Plane Mask the same amount as the OIWFS Steering Mirror.
21. Capture and save science frames. (60 seconds)
22. Offset to the sky position.
23. Capture and save sky frames. (60 seconds)
24. Offset the telescope to the science object.
25. Repeat the object/sky captures 5 times.
26. Change filters and repeat these steps if more wavelengths are required.
27. Pause the AO loop.
28. Offset the telescope to a flux standard position.
29. Reposition the PWFS for flux standard.
30. Turn on the AO loop.
31. Position the star on the same starting pixels as the companion by adjusting the Steering Mirror.
32. Capture and save science frames.
33. Offset the telescope to the sky position.
34. Capture and save sky frames. (60 seconds)
35. Offset the telescope to the science object.
36. Repeat the object/sky capture pair 5 times.
37. Dither the position.

38. Capture and save science frames.
39. Offset to the sky position (use PWFS1 for primary corrections).
40. Capture and save sky frames. (60 seconds)
41. Offset the telescope to the science object (use PWFS1 and PWFS2 for primary corrections).
42. Repeat the object/sky captures 5 times.
43. Repeat the dither 3 more times.
44. Change filters and repeat if more wavelengths are required.

5.6.4 Astrometry

Prime among the NICI science objectives is discovering new companions. Yet the sensitivity limits achievable with NICI are deep enough that often faint detections will be background objects. It is important that an accurate position of the candidate companion be recorded so that follow up work can be done to classify the object and to verify that it is associated with the primary star under investigation.

There are a variety of reasons for wanting to know the candidate companion's position and each has a required accuracy. One key reason for wanting the position would be to allow a follow up spectroscopy measurement. Here the desired accuracy would be a fraction of the spectrograph slit, say around 0.1 arcsecond. Another similar reason would be to communicate the position to others so that they could try to duplicate the image. Again, around 0.1 arcseconds accuracy would be adequate.

A second key reason for wanting the candidate companion's position would be to verify that the companion has the same proper motion as the primary. This is particularly important for objects in large, very slow orbits around the primary. Here the higher the astrometric accuracy the less time is needed to make the measurement. A high proper motion primary would move about a half an arcsecond a year however many target objects would have far less motion. In effect higher astrometric accuracy extends the range of this technique. For this method required accuracy ranges from around a tenth of an arcsecond to as good as can be accomplished.

The third key reason for astrometry is to measure the orbit of the object. A Jupiter-like body orbiting at Jupiter's orbit around a star at 5 parsecs will move about 0.5 arcseconds per year. Larger, slower orbits would move far less. Here the accuracy required depends on the science goals and could range from merely proving that the companion is orbiting the primary to looking for detailed information about the orbit and perturbations of the orbit. Again desired accuracies would range from around 0.1 arcseconds to as good as can be accomplished.
What is the practical limit in astrometric accuracy for NICI? Astrometrists prefer an over sampled PSF with about 3-4 pixels per FWHM. NICI has 3.5 pixels per diffraction core at K so the sampling is well suited to accurate astrometry. Astrometric telescopes with fat seeing limited PSFs are able to centroid to about a few percent of a pixel giving accuracies around a few milliarcseconds. NICI with 18 milliarcsecond pixels should be able to centroid objects to a few milliarcseconds relatively easily. This does not translate to an astrometric accuracy of the same level however.

There are a few challenges with doing astrometry with NICI. First there is some focal plane distortion. This is a result of keeping the optics very simple. This distortion is described in SDN1007 Optical Performance. NICI has field distortion as high as 1.8% at the corner of the field. It is much smaller at the center of the field. This would give astrometric errors as high as 0.23 arcseconds at the corner of the field if not corrected. This can be corrected using the ray trace data or by measuring the distortion by moving a star around in the field.
A second challenge for astrometry with NICI is that the PSF will not be Gaussian. A high Strehl image usually has structure in the PSF. This could cause some centroiding error but is probably offset by the small images and the small pixels.

The primary goal is to achieve astrometric position with respect to the primary and therein lies the largest challenge with NICI. Since NICI occults the primary star and masks the spider flares there is very little light left to process for a centroid. There are four ways listed below to get an accurate position of the primary. Which method is used will depend on the accuracy required and experiments to determine which is most effective. How long it takes to detect the companion will also affect the method used.

5.6.4.1 Methods to get the Centroid of the Primary

1) The easiest method is to use the light that spills around the mask, a donut image. This has been used with CoCo on the IRTF to drive the tip/tilt system with good results. That was with a seeing limited image that was round and fairly uniform with time. The NICI PSF will have more structure and the structure may change with time this could cause a shift in the centroid. The advantage of this method is that the donut image is always there and can always be used without any extra observational steps.

2) The second and probably best method involves moving the focal plane mask out of the way to image the primary directly. Since the dichroic beamsplitter that feeds the AO WFS is before the focal plane mask the mask can be moved without loosing lock in the AO system. There may be some shift when the mask is moved but this can be checked. The mask does not have to be removed entirely, just shifted enough to get the focal plane mask clear of the star. For very long observations this can be done periodically throughout the observation.

3) The third method would be to intentionally misalign the spider mask periodically. The spider flares point to the primary and can be used for determining the position. This method was also used with CoCo data.

4) The forth method would be to use partially transmissive mask. This allows the star to be imaged through the mask at all times. This would probably have to be a hard edge mask since trying to get a centroid of a PSF behind a Gaussian shaped transmissive mask would require modeling or characterization measurements to get an accurate position. The hard edged, partially transmissive mask would have degraded coronagraphic performance but would make accurate astrometry easier. The transmission of the mask would have to be tailored to the brightness of the primary being observed. NICI is not baselined to have any partially transmissive hard edged masks but it will have a user position in the focal plane mask wheel where one can be added for special observations.

Using method number 2, astrometric accuracy is expected to be in the 5 milliarcsecond range as long as the distortion is corrected and this method or method 4 is recommended for the highest astrometric accuracy. Method number 1 should yield accuracies of a pixel or less and can be used when accuracy demands are relaxed.

5.6.5 Other Observing Scenarios

There are 24 filter positions in each imaging channel and positions for 15 possible channel separating elements. These components work together to enable a given observing strategy. There are many possible combinations of filters and dichroics to permit maximum creativity on the part of the observer. We give some descriptions and discussion of other observing scenarios in this section.

a. By using a dichroic to split the beams with bandpass filters downstream in each channel filter wheel one can do simultaneous two color filter radiometry. This is an efficient way to classify a large sample of objects and save valuable telescope time.

b. By using a narrow band filter to divide the channels, in-band information is sent to one channel and all out-of-band to the other. Filters in the individual channels can then shape the out-of-band to make the necessary continuum measurements. For a given spectral line it may be advantageous to sample the continuum by straddling the line, or by measuring longward or shortward of the line. Filter choices will be designed to work with line filters to allow several possibilities for continuum measurement.

c. Several methane-differencing strategies are possible based on H, K and L features. These can be implemented in a variety of ways using either a long/short dichroic split with downstream filters in each channel or using the line itself to generate the split and measuring the continuum as described above.

d. The most important function of the two-channel camera is to permit the rejection of residual background. Because we are observing in the immediate vicinity of the IAO guide object we have no problems with changes in the isoplanatic patch associated with using two separated stars. Because we are observing simultaneously we have no problem with the repeatability of the atmospheric record. But because we are often observing at two different wavelengths, we have a fundamental focal plane scaling issue associated with the wavelength difference. This raises the issue of the best way to scale the two channels onto each other.

e. For line/continuum observations in particular there are several strategies to making the best continuum measurement. It is impossible to say which is best at this time particularly since it is rare that a spectrum consists of a single line in a flat continuum. Where the spectrum has complex structure it will be necessary to have some flexibility in making the continuum measurement. One consequence of the flexibility inherent In the NICI design there are often two ways to make the same observation. For example instead of using a long/short channel split and bandpass filters in each channel one could use a 50/50 neutral density channel split and the same bandpass filters. The latter is less efficient but it is an important verification tool. Furthermore, in this mode, the role of the two channels can be reversed for further confirmation of a given observation.

5.7 Night-time Shutdown

This section is to be written after the instrument has been tested at the Telescope.

5.8 Preliminary Data Reduction

This section is to be written after the instrument has been tested after some data has been taken.

The planned sections would be:

5.8.1 Mapping of Arrays to Each Other

5.8.2 Sky Subtraction and Dark Current Subtraction

5.8.3 Flat Fielding

5.8.4 Frame Differencing

6 Gemini Operation

This section describes operational aspects concerning the Gemini system when making observations with NICI.

6.1 Observing Tool

TODO: Gemini is to write this section per discussions at the Quarterly Review in August 2004.

6.2 Observing with NICI at Gemini

TODO: Gemini is to write this section per discussions at the Quarterly Review in August 2004.

7 Engineering Interfaces

There are few ways NICI can be controlled. The primary method is through the Gemini instrument Sequencer which is described in Section 6. In addition there are engineering interfaces or graphical user interfaces that allow control on the instrument for testing and troubleshooting. These are:

- NICI Engineering Interface also called the IC interface
- AO XUI(X windows based User Interface)
- Array Controller User Interface
- DV, a Fits data viewer

In normal operation at the telescope the Gemini instrument sequencer will control the instrument but the AO system will be monitored using the AO XUI. The AO information is real-time and the data rates are too fast for the EPICS system. The AO user interface displays wavefront curvature data and corrections to the deformable mirror that allows the operator to determine if the AO system is operating properly.

The NICI Engineering Interface and the Array Controller Interface will be used for testing and troubleshooting only. The NICI Engineering Interface will run the entire instrument. The Array Controller Interface will operate only one array controller and may never be used but is included because it may be useful for troubleshooting array or array controller problems.

7.1 Adaptive Optics Interface (XUI) Description

The AO GUI, the XUI, is described in detail in the AO Users Manual, an addendum to this User Manual.

7.2 Instrument Controller (IC) Engineering Interface

The NICI Engineering Interface is described in detail in an addendum to this manual called NICI IC Engineering Interface.

7.3 Array Control Interface

The Array Controller Interface is described in an addendum to this manual in a document called MKIR Array Controller Interface.

7.4 DV: Data Viewing and Arithmetic Operations

The Data Viewer DV is described in an addendum to this manual called the Data Viewer Description.

8 Setup and Operation

8.1 Start-up Procedure

This section is to be written after system testing is complete.

8.2 System Checkout

This section is to be written after system testing is complete.

8.3 Temperature Monitoring While in Use

This section is to be written for the final release of the manuals.

Need to discuss this with Tom.

From SDN2001:

- Required Cold structure temperature: 75K max, Section 3.0
- Required Detector Temperature: 30 - 35 K, Section 4.0
- Required Radiation Shield Temperature: 150K max, Section 5.0.

8.4 Shutdown Procedure

This section is to be written after system testing is complete.

9 Basic Troubleshooting

Per Tom Hayward, this section is to be written during commissioning.

10 Acronyms and Definitions

AO	Adaptive Optics
APD	Avalanche Photo Diode
APSS	Array Power Supply Subsystem
DHS	Gemini's Data Handling System
DM	Deformable Mirror
FITS	Flexible Image Transport System
FOCS	Fiber Optic Calibration Source (in the IAO Relay)
GCU	Gemini Calibration Unit
GND	Electrical ground
HST	Hubble Space Telescope
HVA	High Voltage Amplifier
IAO	Instrument Adaptive Optics system, NICI's AO.
IS	Gemini's Instrument Sequencer
LLA	Lenslet Array
ND	Neutral Density
NDR	Non-Destructive Read
NICI	Near Infrared Coronagraphic Imager
OAP	Off-Axis Parabolic mirror
OCS	Observatory Control System
OIWFS	On-Instrument Wavefront Sensor
PSF	Point Spread Function
PWFS	Peripheral Wavefront Sensor
RT	Real Time
SSA	System Support Associate
UI	User Interface, usually referring to the IAO UI Server.
WFS	Wavefront Sensor

Appendix A: Filter and Mask Physical Specifications

Several of NICI's filter and mask wheels have spare positions which may be populated by Gemini after the instrument is delivered. This section provides the physical specifications of the filters and masks that will be needed for populating the spare positions.

Focal Plane Mask Physical Specifications

Parameter	Value	Tolerance
Surface shape	Plane parallel	wedge +/- 3 arcminutes
Substrate	Calcium Fluoride	
Working temperature	~ 275 K	
Thickness	5.00 mm	+/- 0.05 mm
Physical diameter	35.00 mm	+0.0/-0.05 mm
Clear aperture diameter	11.9 mm	11.9 x 11.9 mm (rect.)
Beam footprint diameter	0.013 mm	
Surface RMS 1	λ/42 over any 1/4 beam footprint	RMS @ 0.63 µm
Surface RMS 2	λ/30 over any 1/2 beam footprint	RMS @ 0.63 µm
Surface RMS 3	λ/21 over any beam footprint	RMS @ 0.63 µm
Surface RMS 4	λ/0.8 over clear aperture diameter	RMS @ 0.63 µm
Sides	Smooth to meet positioning of +/- 0.05 mm	
Surface finish	< 30 Angstroms RMS	
Bevel	standard	
Front surface mask	…	
BBAR coat range	1.0 - 5.5 µm	
BBAR coat av. Refl./surface	< 2.5%	optimize for 1.65 µm

Pupil Mask Physical Specifications

Parameter	Value	Tolerance
Surface shape	Plane parallel	wedge +/- 3 arcminutes
Substrate	Calcium Fluoride	
Working temperature	~ 60 K	
Thickness	5.00 mm	+/- 0.05 mm
Physical diameter	25.00 mm	+0.0/-0.05 mm
Clear aperture diameter	13.0 mm	
Beam footprint diameter	13.0 mm	
Surface RMS 1	λ/66 over any 1/4 beam footprint	RMS @ 0.63 µm
Surface RMS 2	λ/47 over any 1/2 beam footprint	RMS @ 0.63 µm
Surface RMS 3	λ/34 over any beam footprint	RMS @ 0.63 µm
Surface RMS 4	λ/34 over clear aperture diameter	RMS @ 0.63 µm
Sides	Smooth to meet positioning of +/- 0.05 mm	
Surface finish	< 30 Angstroms RMS	
Bevel	standard	
Front surface mask	…	
BBAR coat range	1.0 - 5.5 µm	
BBAR coat av. Refl./surface	< 2.5%	optimize for 1.65 µm

Cryostat Beam Splitter/Dichroic Physical Characteristics

Parameter	Value	Tolerance
Surface shape	Plane parallel	wedge +/- 3 arcminutes
Substrate	Calcium Fluoride	
Working temperature	~ 60 K	
Thickness	6.00 mm	+/- 0.05 mm
Physical size	39.68 x 26.41 mm	+0.0/-0.05 mm
Clear aperture diameter	21.0 mm	21 x 15 mm (ellipse)
Beam footprint diameter	18.0 mm	18 x 13 mm (ellipse)
Surface RMS 1	λ/66 over any 1/4 beam footprint	RMS @ 0.63 μm
Surface RMS 2	λ/47 over any 1/2 beam footprint	RMS @ 0.63 μm
Surface RMS 3	λ/34 over any beam footprint	RMS @ 0.63 μm
Surface RMS 4	λ/32 over clear aperture diameter	RMS @ 0.63 μm
Sides	Smooth to meet positioning of +/- 0.05 mm	
Surface finish	< 30 Angstroms RMS	
Bevel	standard	
Front-side dichroic coat	R > 50%	@45 degree
	T > 50%	@45 degree
Backside BBAR coat	R < 1%, optimize for x μm	@45 degree

Channel 1 and Channel 2 Filter Wheel Physical Filter Specifications

Parameter	Value	Tolerance
Surface shape	Plane parallel	< 10 arcseconds
Substrate	Single substrate (not cemented)	
Angle of incidence	0 degrees	
Working temperature	~ 65 K	
Average transmission	80%	Goal 90%
Trans. half-power point uniformity	+/- 0.5%	
Trans. ripple	< +/- 5% of average transmission	
Slope	< 2.5%	(T90 - T10) / T10
Out of band leak	< 10^{-4} out to 5.6 μm	
Out of band leak	< 10^{-4} down to 0.5 μm	
Thickness	5.00 mm	+/- 0.05 mm
Physical size	29.0 mm	+0.00/-0.05 mm
Clear aperture diameter	24.0 mm minimum	
Beam footprint diameter	13.0 mm	Single focal plane point
Trans. Wavefront Error	λ/66 over any 1/4 beam footprint	RMS @ 0.63 μm
Trans. Wavefront Error	λ/47 over any 1/2 beam footprint	RMS @ 0.63 μm
Trans. Wavefront Error	λ/34 over any beam footprint	RMS @ 0.63 μm
Trans. Wavefront Error	λ/28 over clear aperture diameter	RMS @ 0.63 μm
Surface finish	<30 Angstroms RMS	
Scratch Dig	60/40	
Coating materials	No radioactive materials	

AO Neutral Density Filter Physical Specifications

Parameter	Value	Tolerance
Surface shape	Flat	
Substrate	BK7	
Working temperature	~ 275 K	
Thickness	< 5.0 mm	+/-0.25 mm
Physical size	50.8 mm	+/-0.1 mm
Clear aperture diameter	30.8 mm	
Beam footprint diameter	30.8 mm	
Surface RMS 1	λ/4	RMS @ 0.63 μm
Surface finish	< 30 Angstroms RMS	
Bevel	standard	